INFORMATION TO USERS

This manuscript has been reproduced from the microfilm master. UMI films the text directly from the original or copy submitted. Thus, some thesis and dissertation copies are in typewriter face, while others may be from any type of computer printer.

The quality of this reproduction is dependent upon the quality of the copy submitted. Broken or indistinct print, colored or poor quality illustrations and photographs, print bleedthrough, substandard margins, and improper alignment can adversely affect reproduction.

In the unlikely event that the author did not send UMI a complete manuscript and there are missing pages, these will be noted. Also, if unauthorized copyright material had to be removed, a note will indicate the deletion.

Oversize materials (e.g., maps, drawings, charts) are reproduced by sectioning the original, beginning at the upper left-hand corner and continuing from left to right in equal sections with small overlaps.

Photographs included in the original manuscript have been reproduced xerographically in this copy. Higher quality 6" x 9" black and white photographic prints are available for any photographs or illustrations appearing in this copy for an additional charge. Contact UMI directly to order.

ProQuest Information and Learning
300 North Zeeb Road, Ann Arbor, MI 48106-1346 USA
800-521-0600

UMI®

STATISTICS OF ELECTROMAGNETIC PROPAGATION AND LOCALIZATION

by

ANDREY A. CHABANOV

A dissertation submitted to the Graduate Faculty in Physics in partial fulfillment of the requirements for the degree of Doctor of Philosophy,
The City University of New York

2002

This manuscript has been read and accepted for the Graduate Faculty in Physics in satisfaction of the dissertation requirement for the degree of Doctor of Philosophy.

12/18/01
Date

Professor Azriel Genack
Chair of Examining Committee

1/10/02
Date

/s/ Professor Louis Celenza
Executive Officer

Professor Joseph Birman

Professor Lawrence Ferrari

Professor Alexander Lisyansky

Doctor Victor Kopp

Supervisory Committee

THE CITY UNIVERSITY OF NEW YORK

ACKNOWLEDGMENTS

As in the case with most achievements, the finished work is the result of one man's labor and of many people's help. I owe my advisor Professor Azriel Genack a great debt of gratitude for introducing me to the world of experiment. I appreciate the cooperation and helpful attitude of my colleagues Dr. Mike Kempe, Dr. Victor Kopp, Dr. Marin Stoytchev, Bing Hu, Walter Polkosnik, and Dmitri Zaslavsky. I am grateful to Alex Geyfman, Gregory German, Edward Kuhner, and Zdzislaw Ozimkowski for technical assistance and expertise without which this work would not have been possible.

I would also like to thank the faculty and staff and my student fellows at the Physics Department of Queens College, and especially Professors Fred Cadieu, Lev Deych, Lawrence Ferrari, Alex Lisyansky, Steve Schwarz, Doctors Dmitri Livdan, Victor Podolsky, Yuri Strzhemechny, Alex Yamilov, and Shirley Allen, Donna Hernandez, Susan Wasserman for their continued support. I feel especially grateful towards Professor Narciso Garcia for the encouragement he continuously gave me.

I would like to thank Professors Joseph Birman, Lawrence Ferrari, and Alexander Lisyansky, and Doctor Victor Kopp for serving on the Advisory Committee for my thesis defense.

Finally, I would like to thank my loved Irena and Kostya for their support of my work.

TABLE OF CONTENTS

LIST OF FIGURES

CHAPTER 1
INTRODUCTION

Waves are the means by which we probe our environment and communicate with one another. Their study has expanded from primordial fascination with everyday observations of ripples in a pond and the ocean's waves to the systematic study of sound, light and the full gamut of electromagnetic radiation, and quantum mechanical waves. The field of electromagnetic propagation has grown with the development of the laser to encompass the exploration of nonlinear and quantum optical phenomena in an expanding array of new materials including optical fibers and photonic band gap structures. The joint application of optics and electronics in communications has made photonics a rapidly expanding aspect of modern life. The study of transport in random media has grown apace. It has been spurred in recent years by advances in imaging, by the interchange with electronic mesoscopic physics, and by the expanding range of statistical aspects of propagation that can be measured and computed.

Wave propagation in random media is essentially a statistical problem [1, 2, 3, 4, 5, 6]. For the precise structure of a random sample is not known, the fine-grained variation in intensity of the reflected and transmitted waves cannot be predicted. An example of a random intensity pattern produced in reflection of a helium-neon laser beam from a sheet of white paper is shown in Fig. 1.1. Similar speckle patterns are produced in transmission. Despite the apparently haphazard character of scattered light, the nature of transport in a random medium can be obtained from a statistical characterization of such complex speckle patterns for all incident frequencies and spatial modes for ensembles of statistically equivalent random realizations. An example of a spectral "speckle" pattern of microwave intensity, measured at a point on the output surface of a random sample of polystyrene spheres, is shown in Fig. 1.2. An even more detailed "fingerprint" of the sample is contained in the spatial and spectral variation of the underlying field.

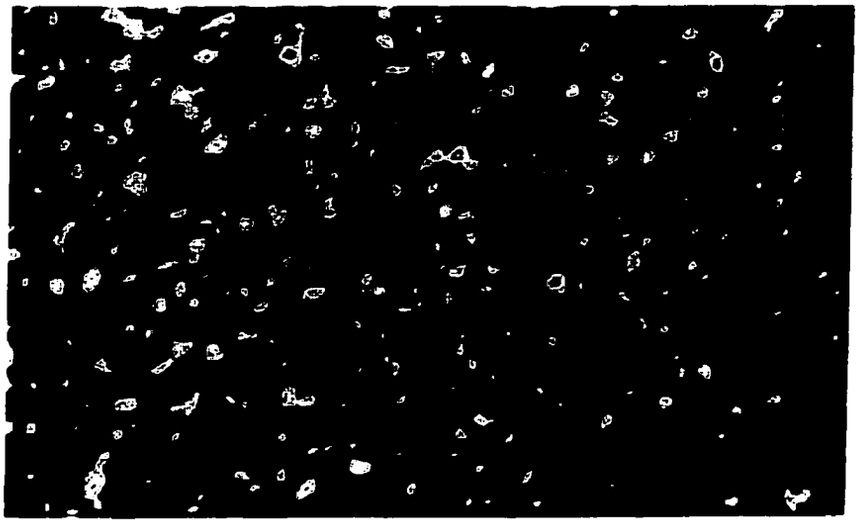

Figure 1.1: The far-field speckle pattern of reflected light is seen in this CCD image of a helium-neon laser beam scattered from a sheet of white paper. Lighter regions have higher intensity. [Photograph courtesy of V. Kopp]

The field is the sum of randomly phased partial waves associated with all possible paths from the source to the point of detection. The field fluctuates with position because of the changing set of partial waves that contribute to the field at different points. The linear superposition of such partial waves corresponds to the sum of phasors shown schematically in Fig. 1.3. Each partial wave may be represented by an arrow or phasor with length proportional to the field amplitude and with phase equal to that of the partial wave. The component of the phasor along the x-axis (y-axis) gives the component of the field, which is in-phase (out-of-phase) with the incident wave. The fluctuations in the field with frequency shift at a given point are primarily due to changes in the phase difference, $\Delta\varphi = 2\pi\Delta s/\lambda$, between partial waves, which differ in path length by Δs, as a result of the change in wavelength λ. Measurements of the microwave field at the same point and in the same random sample realization as in Fig. 1.2 are shown in Fig. 1.4. Both the in-phase and out-of-phase components of the transmitted field, referenced to the field at the input surface, are measured

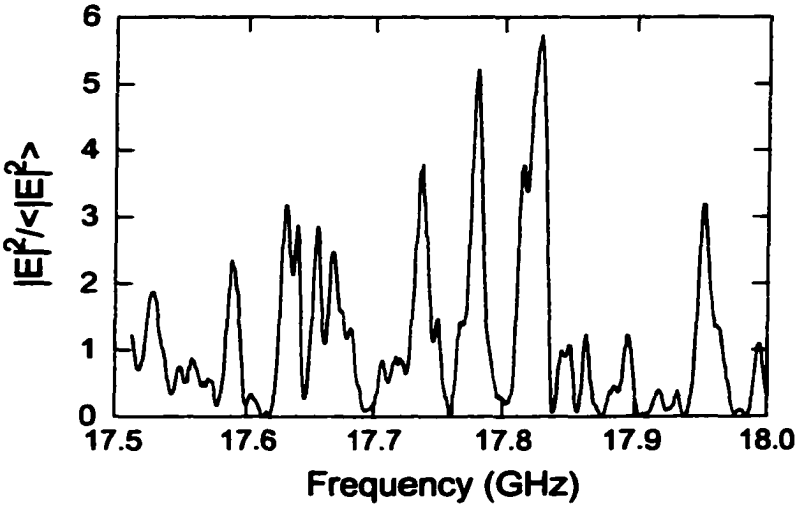

Figure 1.2: Normalized spectrum of the intensity of a single polarization component of the microwave field transmitted through a random collection of 1.27-cm-diameter polystyrene spheres in a 100-cm-long waveguide. Only a single polarization component is detected using a wire antenna positioned at the sample output surface. Its amplitude is squared and divided by the ensemble average of this quantity.

with use of a Hewlett-Packard network vector analyzer. The intensity in Fig. 1.2 is calculated as the sum of the squares of the in-phase and out-of-phase components. The magnitude of the field, $|\mathbf{E}|$, and the phase modulus 2π, ϕ, are computed from these components and the resultant spectra are displayed in Fig. 1.5.

In order to describe the nature of transmission in a random medium, the full probability distributions of transmission quantities should be given rather than their ensemble averages. These distributions reflect correlation in the medium, whose dependence upon position and frequency give key static and dynamic aspects of average transport. Let us consider, for example, correlation functions of the field. The field correlation function with displacement on the sample surface for an ensemble of sample realizations is the Fourier transform of the variation of the ensemble average of

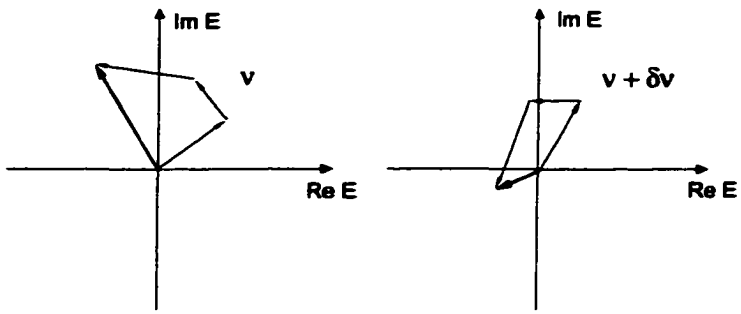

Figure 1.3: Partial waves associated with different trajectories are shown as phasors and summed to give the total field. Each phasor is a complex-valued contribution E with real part corresponding to the in-phase component and imaginary part corresponding to the out-of-phase component of the partial wave.

the far-field intensity with angle [7]. Similarly, the field correlation function with frequency shift is the Fourier transform of the time-of-flight distribution of radiation reaching a point [8, 9]. Thus considerable insight is gained by dealing with field correlation functions, which involve both the amplitude and phase of the wave.

It is often convenient, however, to consider these variables separately. Key aspects of the statistics of steady-state transmission with monochromatic sources can be obtained from measurements of distribution [1, 2, 10, 11, 13, 14, 15, 16, 21, 22, 23, 26, 28, 29, 32, 33, 34, 35, 36, 37, 117, 41, 42, 43, 44, 46] and correlation [15, 17, 18, 19, 20, 22, 23, 24, 25, 27, 30, 31, 42, 46] of the local intensity and spatially averaged flux. At the same time, basic aspects of the statistics of dynamics are revealed by measuring the probability distribution of the spectral derivative of the phase [48, 49, 51, 52, 53, 54, 55, 56, 57, 58, 61, 62, 63, 64, 65, 66, 67]. The derivative $d\phi/d\omega$, where ω is angular frequency, equals the average photon transit time of a narrow band pulse from the source to the detector.

Large fluctuations are a distinctive feature of wave propagation in random media. The nature of fluctuations is determined by the closeness to the localization transition. As a result, the extent of localization can be determined by any of a wide variety of related statistical measurements. In this introductory chapter, we will first discuss

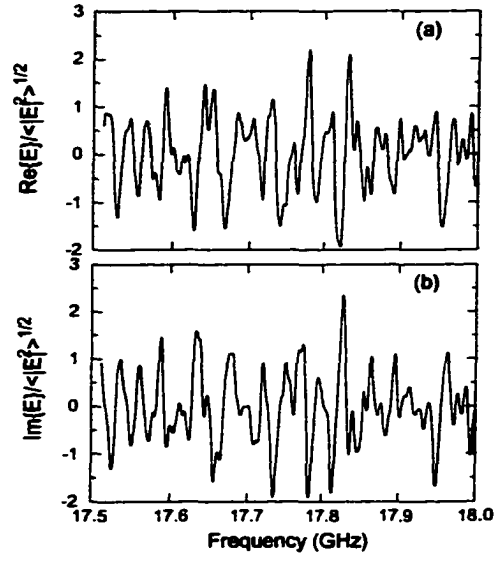

Figure 1.4: The real and imaginary parts of the microwave field at the same point and in the same sample configuration as in Fig. 1.2.

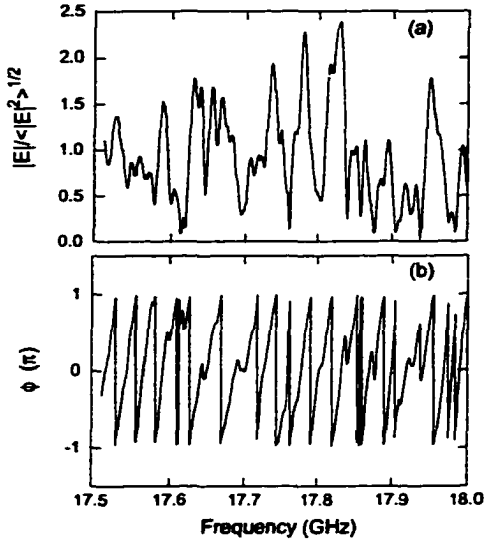

Figure 1.5: The magnitude $|\mathbf{E}|$ normalized to its ensemble average value and the phase modulus 2π, ϕ, of the microwave field calculated using the data in Fig. 1.4.

the statistics of static transmission quantities, emphasizing the relationships between key statistical aspects of propagation in quasi-1D samples. We will also scope the origins and signatures of localization. Then, we will consider the statistical aspects of wave dynamics.

1.1 Fluctuations in steady-state transmission

Making the assumption that the scattered field can be represented as a superposition of a large number of statistically independent partial waves, the probability distribution of the in-phase and out-of-phase components of the amplitude of polarized monochromatic radiation is a gaussian, while the distribution of the phase modulus 2π is flat [2, 37]. The corresponding intensity distribution was calculated by Rayleigh and bears his name [10]. For a given polarization component of the field, the probability distribution of the associated intensity is a negative exponential. When the intensity is normalized to its ensemble average value, its distribution is a universal function independent of the physical dimensions or scattering strength of the sample, $P(s_{ab}) = \exp(-s_{ab})$, where $s_{ab} = T_{ab}/\langle T_{ab}\rangle$. Here T_{ab} is the transmission coefficient or transmitted intensity in mode b for incident mode a, and $\langle ...\rangle$ represents the average of the quantity between the brackets over an ensemble of statistically equivalent samples. Depending upon the experiment under consideration, these modes may correspond to different transverse momentum states of the far field, or to different modes of a microwave cavity, or to the fields within different coherence areas on the sample surface. A schematic representation of key transmission quantities is presented in Fig. 1.6. For this negative exponential distribution for a single polarization component of the radiation, the variance of the normalized intensity is equal to its average value, $var(s_{ab}) = 1$. Since the exponential distribution obtained in the absence of intensity correlation is universal, its measurement provides no information regarding wave propagation beyond the confirmation of the reasonableness of the model, which may apply to a lesser or greater extent in the diffusive limit. However, the average transmission $\langle T_{ab}\rangle$, which is the first moment of the transmission distribution $P(T_{ab})$, depends upon the scattering strength and absorption of the medium, and both the

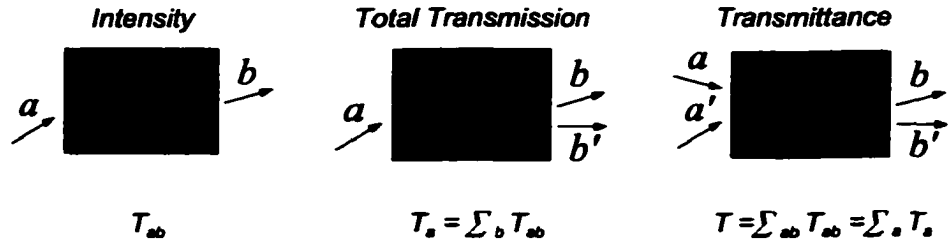

Figure 1.6: Transmission coefficients in random media in order of increasing spatial averaging. The incident and outgoing modes a and b may be in any complete representation of the field.

transport mean free path ℓ and the diffusive absorption length L_a can be determined from the scaling of $\langle T_{ab} \rangle$ with sample length L. In particular, when absorption is absent, $\langle T_{ab} \rangle \sim \ell/L$ [1, 8].

As a result of spatial correlation, however, waves are not statistically independent and deviations from the Rayleigh distribution are observed. The intensity distribution then provides essential information regarding the nature of transport and intensity correlation within a medium. The cumulant correlation function of the normalized intensity is given by $C = \langle \delta s_{ab} \delta s_{a'b'} \rangle$, where, $\delta s_{ab} = s_{ab} - 1$, is the fluctuation from the ensemble average value of s_{ab}. Short-range intensity correlation is associated with field correlation and reflects the inability of a wave to change on a scale much shorter than the wavelength [15]. This short-range component of the cumulant intensity correlation function C is denoted C_1 and is obtained by factorizing the field [15, 17, 42]. Its dependence upon displacement $\Delta\mathbf{R}$, which is given by $C_1(\Delta\mathbf{R}) = |\langle \mathbf{E}(\mathbf{R})\mathbf{E}^*(\mathbf{R}+\Delta\mathbf{R}) \rangle|^2 / \langle |\mathbf{E}(\mathbf{R})|^2 \rangle \langle |\mathbf{E}(\mathbf{R}+\Delta\mathbf{R})|^2 \rangle$, can be computed directly from measurements of the field [45]. It is shown in Fig. 1.7. This term is immediately evident in the speckle pattern of laser radiation, such as that shown in Fig. 1.1. Given an illuminated area A and wavelength λ, the number of transverse modes for a vector wave is equal to the number of speckle spots, $N = 2\pi A/\lambda^2$. Since the number of partial waves associated with distinct paths within the medium, which contribute to the field at a point, greatly exceeds N, these waves must be correlated

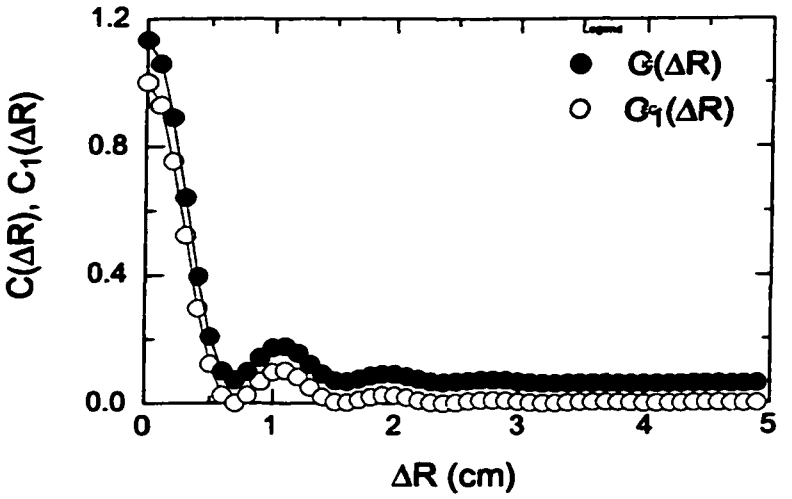

Figure 1.7: The square of the field correlation function with displacement. This is the field factorization contribution C_1 to the normalized cumulant correlation functions with displacement of the intensity, C, for the sample described in Fig. 1.2 and in the text. [From P. Sebbah, R. Pnini, and A.Z. Genack, PRE **62**, 7348 (2000)]

and departures from Rayleigh statistics can be expected. In addition to short-range correlation, scattering in the medium and subsequent diffusion induce intensity correlation across the entire sample. The difference $C-C_1$ gives longer-range contributions to C. Aside from an oscillatory contribution of the same form as seen in Fig. 1.7, $C - C_1$ has a long-range component with displacement. In quasi-1D samples with length L much greater than the transverse dimensions of the sample, the wave is confined by reflecting walls so that the modes are completely mixed. In this case, the long-range contribution to C is constant between points in the transmitted wave [17, 20, 22, 24, 27]. The degree of long-range correlation may be represented by $\langle \delta s_{ab} \delta s_{ab'} \rangle$, where b and b' are points separated by several intervening speckle spots. The main part of the oscillatory component arises from the correlation in the field. The constant background contribution to C is dominated by a term denoted by C_2, which is calculated by including a single crossing of fields in the medium, represented by a Hikami box in a perturbation expansion of the Green function [17, 20]. In the absence of absorption, the degree of long-range correlation is proportional to $L/N\ell$ [17, 20, 22, 24, 27].

The impact of spatial correlation upon distributions of transmission quantities is perhaps most transparent for the distribution of the total transmission for a given incident mode a, normalized by its ensemble average value, $P(s_a)$, where $s_a = T_a/\langle T_a \rangle$. Here, $T_a = \Sigma_b T_{ab}$, is the sum of transmission coefficients over all output modes, as shown schematically in Fig. 1.6. If the intensity at different points were uncorrelated, transmission would be the sum of statistically independent fluxes at an unbounded number of points. The total transmission distribution would then be a delta function. However, as a result of short-range correlation in the intensity, there can be no more than N coherence areas in the transmission speckle pattern. Thus, if there were no correlation in the flux in distinct coherence areas, we would expect that the variance of the normalized total transmission resulting from the sum of N contributions, each of order $1/N$, would be, $var(s_a) = N(1/N)^2 = 1/N$. Instead, for diffusing waves in the absence of absorption, the variance is larger by a factor of L/ℓ, giving $var(s_a) \sim L/N\ell$, which equals the degree of long-range correlation. Thus enhanced fluctuations in transmission are the result of extended spatial correlation and the distribution of the

normalized total transmission reflects the nature of scattering in the medium.

The distribution $P(s_{ab})$ of the normalized intensity in quasi-1D samples can be expressed in terms of the distribution $P(s_a)$ [34],

$$P(s_{ab}) = \int_0^\infty \frac{ds_a}{s_a} P(s_a) \exp(-s_{ab}/s_a). \tag{1.1}$$

This relationship was found in the context of random-matrix theory, and then was confirmed in microwave measurements [41] in random polystyrene samples both with and without the influence of absorption, for diffusive waves and at the localization threshold, as it will be shown below. It is seen from Eq. 1.1, that negative exponential intensity statistics would only be obtained if the distribution of the total transmission were a delta function. But, since spatial correlation is always present to some degree, deviations from Rayleigh statistics are present as well. The intensity distribution displays the extent of this correlation, and hence displays the nature of transport within the sample. Random-matrix theory also gives the relation between the moments of the two distributions, [34]

$$\langle s_{ab}^n \rangle = n! \langle s_a^n \rangle. \tag{1.2}$$

Again, measurements establish that this relation holds independent of the degree of spatial correlation or of absorption of the wave [44].

The existence of intensity correlation at separations well beyond a field coherence length was first recognized in the analysis of fluctuations observed in the electrical conductance of micron-sized samples at low temperatures [12, 13, 14]. Such samples are intermediate in size between the atomic and macroscopic scales and so are termed mesoscopic. The electronic wave function is coherent on a time scale longer than the diffusion time within mesoscopic samples. Hence the field inside the sample is temporally coherent with the incident field. As a result of extended spatial correlation of the current transmission coefficients between any pairs of incident and outgoing modes, the size of conductance fluctuations in mesoscopic conducting samples is enhanced by a factor of $(L/\ell)^2$ and is independent of the scattering strength and sample size [13, 14, 40]. Expressing the conductance as $G = (e^2/h)g$, where e is the electron charge, h is Planck's constant, and g is the dimensionless conductance [74], the vari-

ance of g for mesoscopic samples is 2/15 [20]. Using Landauer approach [77], g can be defined as the transmittance, that is, the sum of transmission coefficients connecting all incident and outgoing modes, $g \equiv T = \Sigma_{ab} T_{ab}$ [78], as illustrated in Fig. 1.6. In the following, we will also use the notation g to denote the ensemble average of the dimensionless conductance.

This incoherent sum is appropriate for physical measurements of conductance, in which temporal averages are taken over times long compared to the phase coherence time of incident current modes. Expressing g or, equivalently, T in terms of the total transmission, $T = \Sigma_a T_a$, one obtains, $g = \langle T \rangle = N\ell/L$, for diffusive waves in the absence of absorption. Thus, $var(s_a) \sim \langle \delta s_{ab} \delta s_{ab'} \rangle \sim 1/g$, suggesting a relationship between fluctuations of total transmission, spatial correlation of intensity, and average transport. Universal conductance fluctuations for diffusive waves corresponds to $var(g) \simeq 2/15$ or, equivalently, $var(s) \simeq 2/15g^2$, where $s = T/\langle T \rangle$. This enhancement arises from the equal extent of correlation of transmission coefficients T_{ab} for all input and output modes associated with a double crossing of fields in the medium, represented by a term in perturbation theory which includes two Hikami boxes. The contribution to C of this term is proportional to $1/g^2$ and is referred to as C_3 or infinite-range correlation [20, 42]. Unlike the short-range C_1 term whose spatial variation is multiplicative in displacement of the source and detector, and the C_2 term which is additive in this regard, the C_3 term is independent of displacement of either the source or detector. The cumulant intensity correlation function is thus given by $C = C_1 + C_2 + C_3$.

1.2 Signatures of localization

A sharp divide exists in the nature of wave propagation [79]. On one side, average transport is not appreciably influenced by wave interference. The wave moves a distance, $\ell \gg \lambda$, before being randomized in direction and, on scales much larger than ℓ, the intensity or charge density follows a diffusion equation. This leads to a transmission coefficient, $T_{ab} \sim \ell/L$, on length scales shorter than the diffusive absorption length, $L_a = \sqrt{D\tau_a}$ [8], where $D = \frac{1}{3} v_E \ell$ is the diffusion coefficient, v_E is

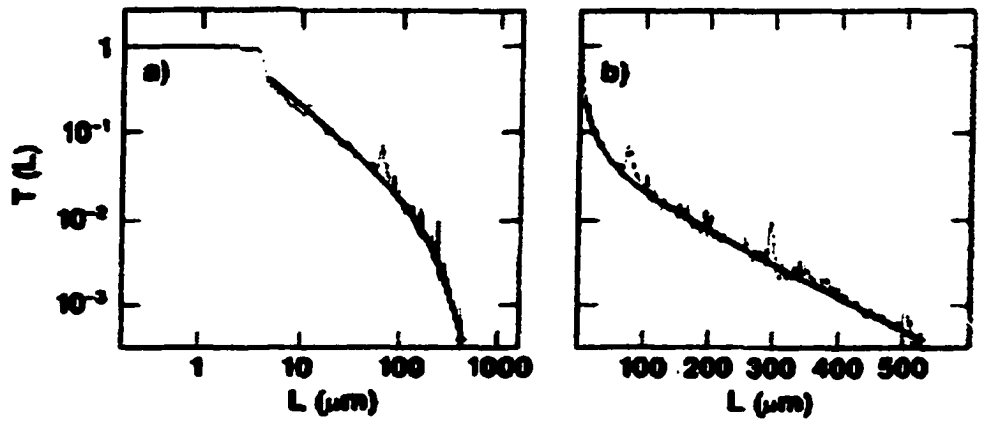

Figure 1.8: (a) Log-log and (b) semi-log plots of normalized optical transmission through a wedge of rutile titania powder in a polystyrene matrix. The plots show the inverse and exponential attenuation of transmission with L for L smaller than and greater than L_a, respectively. [From A.Z. Genack, PRL 58, 2043 (1987)]

the energy transport velocity [80, 81], and τ_a is the absorption time. For $L > L_a$, the wave is attenuated exponentially. The scale dependence of transmission through a wedge-shaped sample of random titania particles dispersed in polystyrene is shown in Fig. 1.8 [8]. The curve gives the fit of the envelope of the data to diffusion theory. The correlation function of intensity with frequency shift measured in the far field is found to coincide with the square of the Fourier transform of the measured time-of-flight distribution [9]. Hence it corresponds to the C_1 contribution to C. For diffusive waves, the degree of intensity or current correlation is small, and so, $var(s_{ab}) \sim 1$, and $var(s_a) \ll 1$.

On the other side of the divide, the constructive interference of waves returning to a point leads to a suppression of transport. The enhancement of intensity in the backscattered direction in a cone of angular width $1/k\ell$, where k is the wavenumber, may be viewed as a precursor to localization [82, 83, 84, 85]. The coherent backscattered cone is the Fourier transform of the point spread function on the input surface. Thus it broadens as the wave is more strongly confined. Such backscattering evidently

becomes large, when $k\ell \sim 1$. The wave then cannot be envisioned as propagating with well defined wavelength between scattering centers, and the particle diffusion picture breaks down [86].

Localization by disorder was first studied in the electronic context, in which disorder is widespread. Anderson [70] showed that electrons on an atomic lattice with disorder in the site energy become localized when this disorder exceeds the off-diagonal coupling between neighboring sites. The wave functions then fall exponentially in space, and transport is absent in unbounded samples. In bounded samples, however, electrons may flow through the sample as a result of exponential coupling to the boundary. The Ioffe-Regel criterion [86] for the breakdown of diffusive, particle-like propagation, $k\ell \sim 1$, suggests the wave origin of the localization transition. This was further elaborated by John *et al.* [75, 76], who argued that classical waves could be localized as well.

Edwards and Thouless [71] argued that electrons would be localized when electron states in a block of material could not be shifted into resonance with a neighboring block as a result of interactions at the sample boundary. One measure of the coupling at the boundary is the level width induced by the coupling of the wave to the boundary, δE. Equivalently, the level width may be expressed in frequency units as $\delta\nu = \delta E/h$. The level width $\delta\nu$ may be identified with the inverse of the particle dwell time within the sample block. It may also be quite naturally defined as the correlation frequency, which is the width of the field correlation function with frequency shift [72]. When $\delta\nu$ falls below the frequency spacing between the levels in equivalent blocks, $\Delta\nu$, which is the inverse of the density of states in the block, the coupling between adjacent blocks of material is inhibited [73]. The lines associated with consecutive levels in two blocks of material, that may be brought together, are shown schematically in Fig. 1.9. Abrahams *et al.* [74] reasoned that, when the dimensionless ratio, $\delta = \delta\nu/\Delta\nu$, is below unity, this quantity will fall exponentially as the sample is scaled up in size. Using the Einstein relation, $\sigma = e^2 D(dn/dE)$, where σ is the conductivity, D is the diffusion coefficient, and dn/dE is the density of states per unit volume, it can be shown that, $g = \sigma A/L = \delta$ [74]. Since the scaling of $g = \delta$ depends upon nothing but the degree of overlap of levels in adjacent blocks of

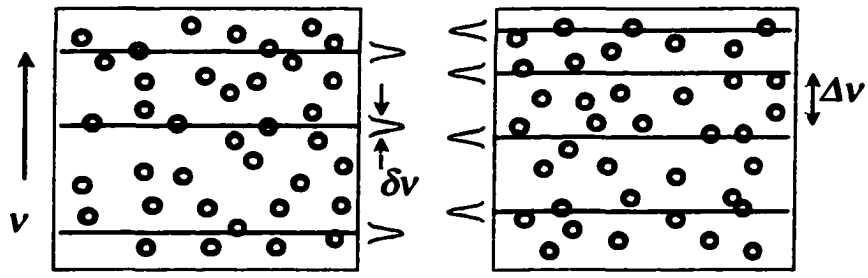

Figure 1.9: Schematic representation of the (mis)matching of modes in two adjacent blocks of a random medium. Here the level width $\delta\nu$ is smaller than the typical level spacing $\Delta\nu$.

material, which is given by δ, it was argued that g is a universal scaling parameter whose scaling depends only upon the value of g [74]. For localized waves, average transmission quantities scale exponentially. Because fluctuations in conductance may be significant, especially for localized waves, scaling relations cannot refer to the value of g for some particular sample realization. Rather they must relate to the ensemble average value of g.

In contrast to the exponential scaling of g for localized waves, the conductance scales as A/L in conducting samples. Both g and δ increase with this scaling factor, as the sample size increases proportionately in three dimensions. Thus, g increases as all dimensions are increased for conducting samples, and g falls for localized samples. The threshold for localization in three dimensions occurs at the fixed point for the scaling of conductance, at which the level width remains equal to the level spacing, i.e. $\delta = g = 1$, as the sample size increases. At the localization threshold, the corresponding transmission for a cube scales as, $T_a = g/N \sim 1/(kL)^2 \sim (\ell/L)^2$ [74].

From the foregoing it is clear that the nature of transport in electronic samples is reflected in the scaling of conductance. The scaling of conductance at the localization threshold and for localized waves requires that the wave function be coherent throughout the sample. However, the A/L type of the scaling holds in conducting samples even in the presence of inelastic scattering. The situation is less clear cut,

however, for classical waves because the number of particles associated with the field is not conserved [76, 87, 88, 89, 90, 95]. The particle number may be reduced by absorption or augmented by gain. We have seen that in the presence of absorption, for example, transmission falls exponentially for $L > L_a$. Thus exponential decay of transmission is not an unambiguous sign of photon localization.

An example of transmission of a classical wave in a strongly scattering sample is shown in Fig. 1.10 [91, 92]. The figure gives the scale dependence of microwave transmission in mixtures of aluminum and Teflon spheres with the same diameter of 0.47 cm at 19 GHz. At an aluminum sphere volume filling fraction of $f = 0.20$, transmission decays inversely with length, from $L = 1$ cm to $L = 7$ cm, indicating diffusive transport. At $f = 0.30$, transmission falls inversely with L^2, suggesting that the localization threshold is reached. An accurate absolute determination of transmission was not made, but g was of the order of unity in this sample for $L < 7$ cm. At a higher concentration of $f = 0.35$, transmission falls exponentially, suggesting the wave is localized. But the possibility that absorption influences transport could not be ruled out.

In more recent experiments, Wiersma *et al.* [93] found a transition from $1/L$ to $1/L^2$ to an exponential in the thickness dependence of infrared transmission in a wedge of GaAs particles, as the size of particles was changed. The wavelength was in the band gap of GaAs, so that low absorption was expected. A broadening of the coherent backscattering peak indicated a small value for the transport mean free path ℓ. However, even small absorption rates can dramatically influence the point spread function on the input face, and the possibility that these measurements were influenced by residual absorption has been raised [95]. One interesting feature of the measurements [93] is that in a sample, where $1/L^2$ scaling of transmission was observed, the value of g for a cubic region of the sample with sides equal to the sample thickness L is significantly larger than unity. This is seen by multiplying the number of modes in an area L^2 by the measured transmission coefficient.

Exponential decay in optical transmission in a sample with low absorption has also been observed recently by Vlasov *et al.* [96] in a nearly periodic opal structure. Again, the value of g was much larger than unity for a cubic region of the sample

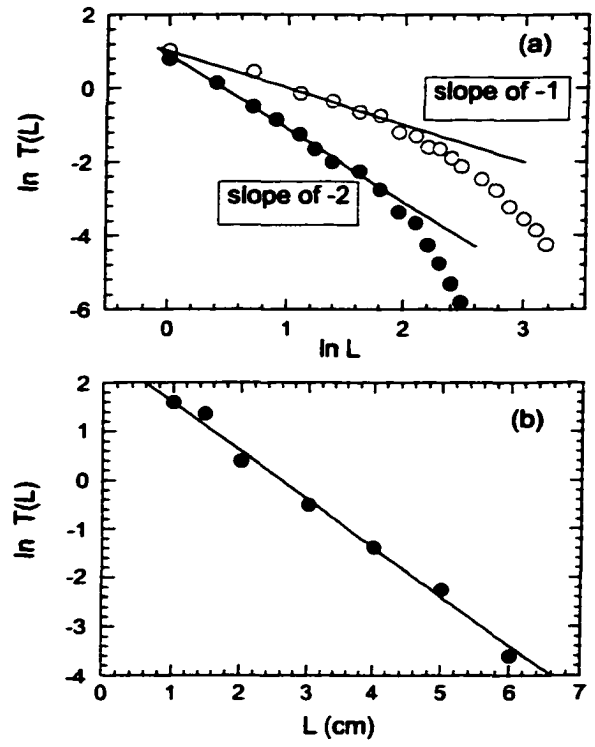

Figure 1.10: Scale dependence of relative transmission for three volume fractions f of aluminum spheres in mixtures with Teflon spheres: (a) in samples with $f = 0.20$ (circles), transmission falls inversely with L, whereas it falls inversely with L^2 in samples with $f = 0.30$ (filled circles); (b) in samples with $f = 0.35$, transmission falls exponentially. The variation of the scaling of transmission is the same as that expected for a transition from diffusive to critical to localized waves in the absence of absorption. [From N. Garcia and A.Z. Genack, PRL **66**, 1850 (1991); PRL **66**, 2064 (1991)]

for small values of L. The exponential fall-off of transmission in this case might be related to the evanescent nature of the wave in the nearly periodic structure.

Recently, van Tiggelen *et al.* [97] have shown that transport, which is renormalized by constructive interference of waves returning to a given point, may be described by an effective position-dependent diffusion coefficient $D(\mathbf{r})$. In contrast to the conventional description of scaling [74] that treats the scale dependence of transport phenomenologically, via a scale-dependent diffusion coefficient $D(L)$, this approach explicitly treats the variation of the effect of interference upon position. Thus, because the probability of return of a wave to a point near the surface is smaller than for a point in the middle of the sample, $D(\mathbf{r})$ increases from the boundary to the middle of the sample. This approach preserves the scaling of transmission for large L. It may, however, lead to enhanced transmission, particularly in the case of samples with internal reflection. In this case, photons that are scattered back to the front surface are reinjected into the sample and transmission is thereby enhanced.

Because of the existence of a variety of explanations for the observations of exponential decay in transmission of electromagnetic radiation, the scaling of the average transmission taken by itself is not an unambiguous indication of localization. Below we will consider other measures of localization and, in particular, statistical measures of fluctuations in transmission. We should note, however, that indications of localization from measurements of average transport and of fluctuations in transport are not necessarily equivalent, even in the absence of absorption. Until recently, it was believed that the value of the conductance or, equivalently, the Lyapunov exponent, $\gamma = -\langle \ln(g)/L \rangle$, which is the inverse of the localization length ξ, can give the magnitude of relative fluctuations in conductance [98, 99]. In single-parameter scaling theory, the magnitude of fluctuations is given in terms of average conductance via the relation, $var(\ln(g)/L) = -2\gamma/L$. But this relation can be violated, as is found in 1D random systems, when the typical distance between localization centers is smaller than the localization lengths of these states, allowing their wave functions to overlap [100, 101].

We have seen that an important aspect of electromagnetic transport, which is not present for electrons, is absorption. The role of absorption is quite different from de-

phasing, since absorption does not lead to a reduction of interference of backscattered waves but simply reduces the amplitude of these waves. It was shown in simulations of acoustic waves on a two-dimensional lattice that a localized acoustic excitation remains localized in space when dissipation is introduced [87]. The impact upon localization of absorption is not accurately represented by its effect on the conductance. Absorption suppresses transmission, and hence transmittance or conductance; at the same time, it weakens the effect of localization. But a reduction of conductance is ordinarily seen as a sign of the strengthening of localization. We therefore seek an indicator of localization, which accurately gives the proximity to the localization threshold in samples both with and without absorption. Similarly, the presence of gain may change the relation between average transport and fluctuations, and an appropriate localization parameter is required in this case.

We also note that, in the presence of absorption, g and δ are affected differently. Whereas g falls, δ increases since the lines broaden due to absorption. Thus these parameters do not reflect the state of transport in the same way. Though we expect that an additional parameter is added when absorption is present, we still seek a parameter that indicates the extent of localization effects.

1.3 Statistics of wave dynamics

Though until recently the focus of mesoscopic physics in all its varieties has been almost exclusively on steady-state propagation, it is natural to view transport from a dynamical perspective. Indeed, the fundamental dimensionless ratio in the study of propagation and localization, the Thouless number δ, is the ratio of two dynamical parameters, the level width $\delta\nu$ and the level spacing $\Delta\nu$, $\delta = \delta\nu/\Delta\nu$ [73]. The level width is the inverse of the Thouless time which is the transit time through the sample, and the level spacing is the inverse of the Heisenberg time which is the time required to explore all coherence volumes of the sample. The statics and dynamics of transport are closely related since, in the absence of inelastic processes, δ is equal to the dimensionless conductance g, which is the inverse of the degree of long-range intensity correlation [17, 20, 24].

Whereas static aspects of transport are associated with the amplitude of the wave, dynamics is reflected in the phase [47, 48, 49, 57, 58]. The single-channel delay time for a transmitted pulse in mode b for incident mode a is the first temporal moment of the pulse, $\tau_{ab} = \int dt I_{ab}(t)t / \int dt I_{ab}(t)$, where $I_{ab}(t)$ is the time-dependent transmission coefficient. In the limit of vanishing pulse bandwidth, the single-channel delay time is found to approach the spectral derivative, $\tau_{ab}(\omega) = d\phi_{ab}(\omega)/d\omega \equiv \phi'_{ab}$, where $\phi_{ab}(\omega)$ is the phase accumulated by the field as it propagates through the sample [57, 58]. In the same limit, the pulse transmission coefficient, $\varepsilon_{ab} = \int dt I_{ab}(t)$, is equal to the static transmission coefficient or intensity $I_{ab}(\omega)$.

The concept of delay times was first discussed by Eisenbud [47] and Wigner [48] as ways of quantifying the lifetimes of metastable states and particularly the duration of collisions. Later, Smith [49] has introduced the delay matrix to treat the many-channel problem. Statistical aspects of dynamics have been considered in nuclear and atomic scattering [49] and in chaotic cavities [52, 53, 54, 55, 56]. Recently, the coherence of classical waves has been exploited to study the statistics of dynamics for diffusing [61, 62] and localized waves [67].

The mesoscopic physics of dynamics reflects the interaction between the single-channel delay time and the intensity. For diffusing waves, the interplay between ϕ'_{ab} and I_{ab} can be seen in that singularities in ϕ'_{ab} are most likely to occur at nulls in the transmitted intensity speckle pattern, since both the in-phase and out-of-phase components of the field vanish there. The phase jumps by π when moving through a null in the speckle pattern. Thus the magnitude of ϕ'_{ab} can be particularly large for low values of the intensity when nulls in the speckle pattern pass near a detector [58]. Strong correlation between delay time and intensity can also be seen by considering the single-channel delay time weighted by the intensity, $W_{ab} = \phi'_{ab}T_{ab}$ [49], which is the appropriate quantity for spatial averages of the delay time. For example, the average delay time in mode a is given by $W_a = (1/N)\Sigma_b \phi'_{ab}T_{ab}$, and the sum over all pairs of modes, $W = (1/2N)\Sigma_{ab}\phi'_{ab}T_{ab}$, is the Wigner delay time, which is proportional to the photon density of states [60]. The quantities W_a and W can be seen as the dynamic equivalents of the total transmission T_a and transmittance T, respectively. In static measurement, the infinite-range contribution C_3 to correlation between transmission

coefficients T_{ab} for all the input and output modes gives rise to universal conductance fluctuations. Since conductance fluctuations are correlated with fluctuations in the photon density of states [68, 69], a C_3 contribution to correlation between W_{ab} is also expected to exist. Further, the corresponding C_2 contribution to dynamic correlation should give rise to enhanced fluctuations in the weighted delay time averaged over output modes, W_a, and is, in fact, seen in the frequency correlation function of W_{ab} [62].

Because of the interplay between statistics of ϕ'_{ab} and I_{ab}, the statistics of local dynamics are best expressed in terms of the joint probability function $P(\phi'_{ab}, I_{ab})$. A universal distribution $P(\hat{\phi}', \hat{I})$, given in terms of the single-channel delay time and intensity normalized to their ensemble average values, $\hat{\phi}' \equiv \phi'_{ab}/\langle\phi'_{ab}\rangle$ and $\hat{I} \equiv I_{ab}/\langle I_{ab}\rangle$, respectively, was found from C_1 theory based upon field correlation [61, 62]. According to the theory, the conditional distribution $P_{\widehat{I}}(\widehat{\phi}')$ for a fixed value of $\widehat{I}$, in the diffusive limit, is a gaussian with a variance equal to $Q/2\widehat{I}$, where the parameter Q is a function only of the ratio of L and the diffusive absorption length L_a [62],

$$Q = \frac{x^2 - 2\sinh(x)^2 + (1/2)x\sinh(2x)}{x\cosh(x) - \sinh(x)}, \tag{1.3}$$

where $x = L/L_a$. In the diffusive limit, the distribution $P_{\widehat{I}}(\widehat{\phi}')$ is centered at $\widehat{\phi}' = 1$ for all values of $\widehat{I}$, and thus the first moment $\langle\widehat{\phi}'\rangle_{\widehat{I}}$ of this distribution is independent of $\widehat{I}$. As a result, the first joint moment $\langle\phi'_{ab}I_{ab}\rangle$, which is also the ensemble average of the weighted delay time W_{ab}, factorizes, $\langle W_{ab}\rangle = \langle\phi'_{ab}\rangle\langle I_{ab}\rangle$. The distribution $P(\hat{\phi}')$ of the normalized single-channel delay time is obtained from $P(\hat{\phi}', \hat{I})$ by integrating $\hat{I}$ out,

$$P\left(\widehat{\phi}'\right) = \frac{1}{2}\frac{Q}{\left[Q + (\widehat{\phi}' - 1)^2\right]^{3/2}}. \tag{1.4}$$

It is centered and symmetrical about $\widehat{\phi}' = 1$, and decays algebraically at large $\widehat{\phi}'$. In contrast, the distribution $P(\widehat{W})$ of the normalized weighted delay time, $\widehat{W} \equiv W_{ab}/\langle W_{ab}\rangle$, which is also obtained from $P(\hat{\phi}', \hat{I})$, is a double-sided exponential and

centered at $\widehat{W} = 0$,

$$P(\widehat{W}) = \frac{1}{\sqrt{Q+1}} \exp\left(\frac{-2|\widehat{W}|}{\theta(\widehat{W}) + \sqrt{Q+1}}\right). \tag{1.5}$$

Surprisingly, measurements of the distribution $P(\widehat{\phi}')$, of the joint distribution $P(\widehat{I}, \widehat{\phi}')$, and of the spectral cumulant correlation function of $\widehat{\phi}'$, $C_{\widehat{\phi}'}(\Delta\omega)$, for diffusing waves were in excellent agreement with theory, even in samples with a considerable degree of long-range intensity correlation [61, 62]. In Fig. 1.11, the distribution $P(\hat{\phi}')$ of Eq. 1.4 is compared to that obtained in an ensemble of polystyrene samples and excellent agreement between the two curves is seen over 7 decades of $P(\hat{\phi}')$ [61, 62]. This indicates weak sensitivity of the statistics of $\hat{\phi}'$ to long-range correlation in these samples. However, extended spatial correlation had a considerable impact on the distribution and correlation of the intensity $\widehat{I}$ and of the normalized weighted delay time $\widehat{W}$ [61, 62].

The statistics of dynamics of localized waves must differ fundamentally from those for diffusing waves, since the transmission spectrum appears as a series of narrow spikes [44], reflecting the condition, $\delta\nu < \Delta\nu$. Unlike diffusive waves, for which the delay time and intensity are uncorrelated [61, 62], long delay times for localized waves are associated with peaks in the transmitted intensity, associated with resonant tunneling through localized states. Calculations of novel statistics of dynamics in localized media have been carried out for reflection of acoustic waves in 1D systems, such as the earth's crust [50], for reflected [63, 64, 65] and transmitted [66] electromagnetic waves in quasi-1D media, and for electron transport in a 1D potential [59]. The statistical dynamics of localized microwave radiation in quasi-1D media have been studied in [67].

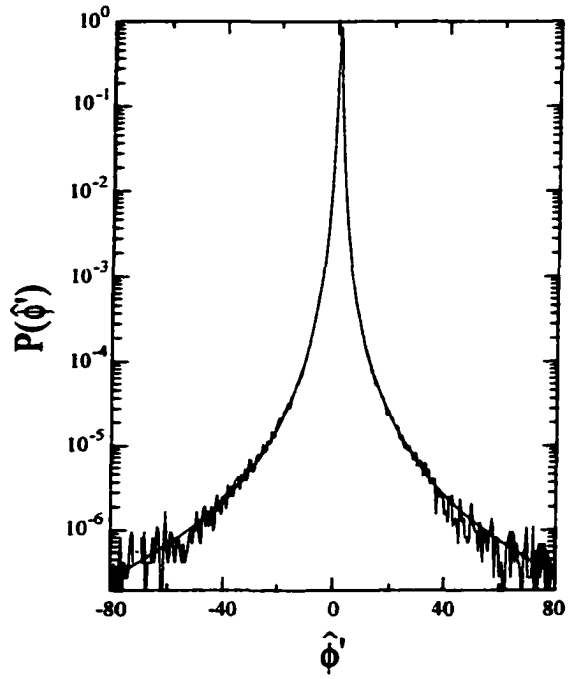

Figure 1.11: Probability distribution function $P(\hat{\phi}')$ of the normalized single-channel delay time. The smooth solid line is the theoretical prediction of Eq. 1.4 using the measured value $Q = 0.31$. [From A.Z. Genack, P. Sebbah, M. Stoytchev, and B.A. van Tiggelen, PRL **82**, 715 (1999)]

CHAPTER 2
STATISTICAL SIGNATURES OF PHOTON LOCALIZATION

To date, claims of three-dimensional photon localization have been based on observations of the exponential decay of the electromagnetic wave [91, 92, 93, 94, 96] as it propagates through the disordered medium. But these reports have come under close scrutiny because of the possibility that the decay observed may be due to residual absorption [87, 89, 95], and because absorption itself may suppress localization [76]. In this chapter, we show that the extent of photon localization can be determined by a different approach – measurement of the relative size of fluctuations in the total transmission or local intensity. The variance of relative fluctuations accurately reflects the extent of localization, even in the presence of absorption. Using this approach, we demonstrate photon localization in both weakly and strongly scattering quasi-1D dielectric samples and in periodic metallic wire meshes containing metallic scatterers, while ruling it out in three-dimensional samples of aluminum spheres.

2.1 Weakly scattering quasi-1D dielectric samples

The first measurements of the distribution of total transmission were carried out by De Boer *et al.* [32] in optical studies in slabs of titania particles. Samples with $g > 10^3$ were studied and the distribution was found to be a gaussian to within 1%. A measure of the deviation of the distribution from a gaussian is the value of the third cumulant $\langle s_a^3 \rangle_c$, which gives the skewness of the distribution and vanishes for a gaussian distribution. For the samples studied, $\langle s_a^3 \rangle_c$ was of order 10^{-6}.

Considerably greater deviations were observed by Stoytchev and Genack [38] in measurements of the probability distribution of total transmission of microwave radiation in quasi-1D samples of polystyrene spheres. The distributions of normalized total

transmission, $P(s_a)$, for three ensembles of samples with different external dimensions are shown in Fig. 2.1. In the absence of absorption, the dimensionless conductance, $g = N\ell/L$, would be approximately 15.0, 9.0, and 2.25 for the samples a, b, and c, respectively. The distributions are markedly non-gaussian, and the deviations from gaussian become more pronounced as either the sample length increases or the sample diameter decreases. A value of $\langle s_a^3 \rangle_c$ as large as 0.112 ± 0.003 was found for the sample c. Deviations from gaussian in the tail of the distributions can be seen in the semi-logarithmic plot in Fig. 2.1b. For large s_a, the distributions have exponential tails.

Since the distributions of intensity and of total transmission are affected by absorption, $P(s_a)$ cannot be simply related to g. But, it was found in these strongly absorbing samples that the distribution $P(s_a)$ can be well expressed in terms of a single parameter $var(s_a)$, or equivalently $g' = 2/3var(s_a)$. In the absence of absorption and in the limit, $g \gg 1$, the full distribution of transmission is given by [33, 34]

$$P(s_a) = \int_{-i\infty}^{i\infty} \frac{dx}{2\pi i} \exp\left(xs_a - \Phi(x)\right), \tag{2.1}$$

where

$$\Phi(x) = g \ln^2(\sqrt{1 + x/g} + \sqrt{x/g}) \tag{2.2}$$

is the generating function. It follows from Eqs. 2.1 and 2.2 that $var(s_a) = 2/3g$, and hence $P(s_a)$ can be expressed in terms of $var(s_a)$ as well as of g. Plots of $P(s_a)$ of Eq. 2.1, obtained after substituting measured values of $var(s_a)$ into Eq. 2.2, are shown as the solid lines in Fig. 2.1b. They are in excellent agreement with the measured transmission distributions. This suggests that $var(s_a)$ is the essential parameter describing transmission fluctuations in random media, even in the presence of absorption. Since the distribution $P(s_{ab})$ of the normalized intensity is given by Eq. 1.1, $var(s_a)$ is characteristic for statistics of transmitted intensity as well.

The assumptions underlying Rayleigh statistics for transmitted intensity in non-absorbing samples can be expressed by the condition, $g \gg 1$. Deviations in the tail of the distribution $P(s_{ab})$ were observed in microwave experiments in samples with $g \approx 10$ [23, 29] and related to the degree of spatial intensity correlation. Corrections to the

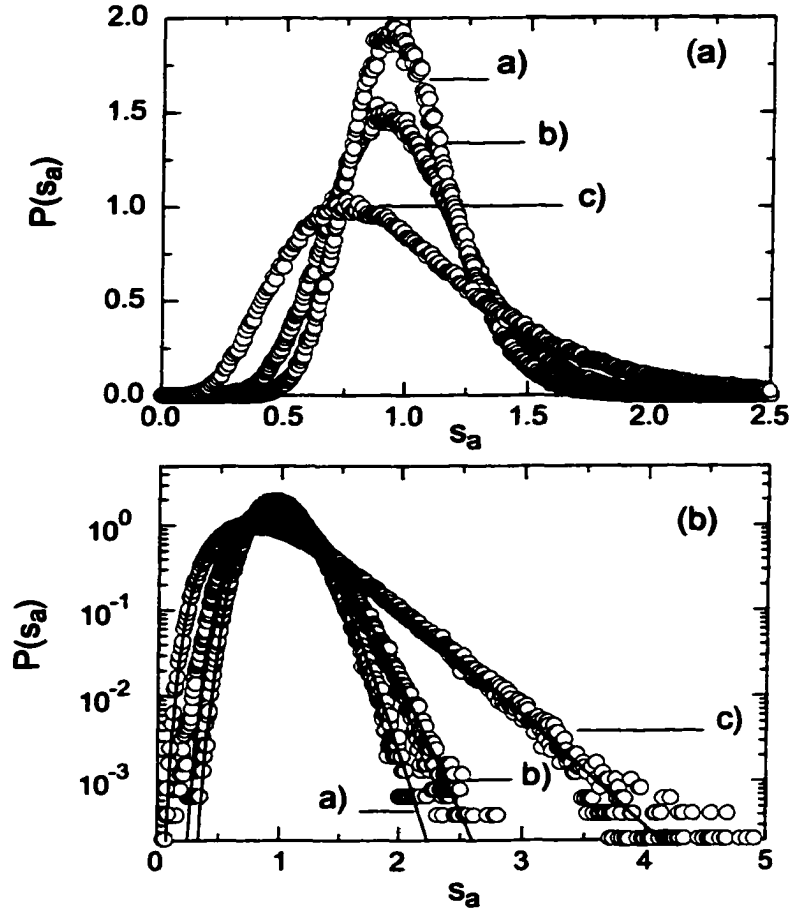

Figure 2.1: Linear (a) and semi-logarithmic (b) plot of the distribution function of the normalized transmission, $P(s_a)$, for three polystyrene samples with dimensions: a) $d = 7.5$ cm, $L = 66.7$ cm; b) $d = 5.0$ cm, $L = 50$ cm; c) $d = 5$ cm, $L = 200$ cm. Solid lines in (b) represent theoretical results obtained from Eq. 2.1, with measured values of g' substituted for g in Eq. 2.2. [From M. Stoytchev and A.Z. Genack, PRL **79** 309 (1997)]

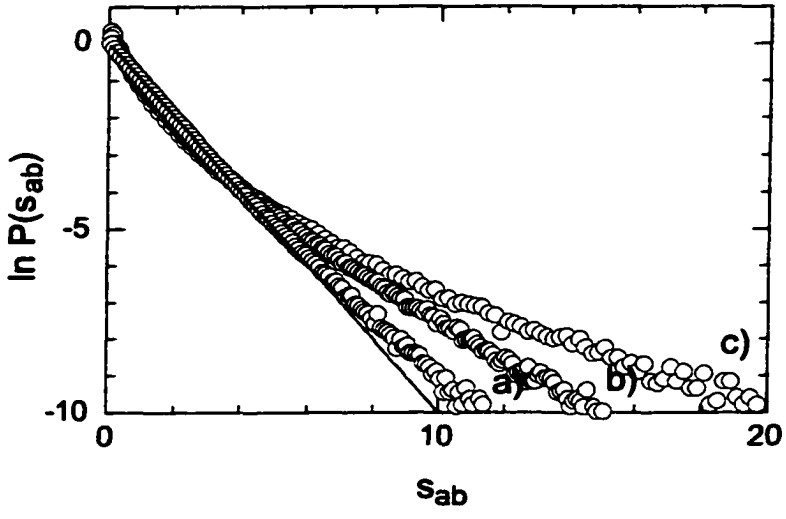

Figure 2.2: Normalized intensity distribution $P(s_{ab})$ for three polystyrene samples with dimensions: *a*) $d = 7.5$ cm, $L = 66.7$ cm; *b*) $d = 5.0$ cm, $L = 200$ cm; *c*) $d = 5.0$ cm, $L = 520$ cm. The Rayleigh distribution is shown as the solid line. [From M. Stoytchev and A.Z. Genack, Opt. Lett. **24**, 262 (1999)]

Rayleigh distribution were calculated by Nieuwenhuizen and van Rossum [33] and by Kogan and Kaveh [34]. They found that the distribution has a stretched exponential tail, $P(s_{ab}) \sim \exp(-2\sqrt{gs_{ab}})$, for $s_{ab} \gg g = \xi/L$. Similar behavior, but with $g' = 2/3var(s_a)$ substituted for g, was found in strongly absorbing samples. Measurements of the intensity distribution of microwave radiation in quasi-1D polystyrene samples with lengths up to L equal to the localization length, $\xi = N\ell$, were reported in [41]. The distributions $P(s_{ab})$ measured in ensembles of three different samples are presented in the semi-logarithmic plot in Fig. 2.2. For the sample *a*, in which $L/\xi = 1/15$, the distribution is close to a negative exponential. But, as L/ξ increases, deviations from Rayleigh statistics increase. To study the tail of the normalized intensity distribution $P(s_{ab})$, for $s_{ab} \gg \xi/L$, theory [33, 34] was fit to the measured distributions using g' as a free parameter. The result of the fit for the sample *b* is presented as a dotted line in Fig. 2.3. For samples, for which $P(s_a)$ was also measured, the values of the fitting parameter g' were found to be within 10% of the values of

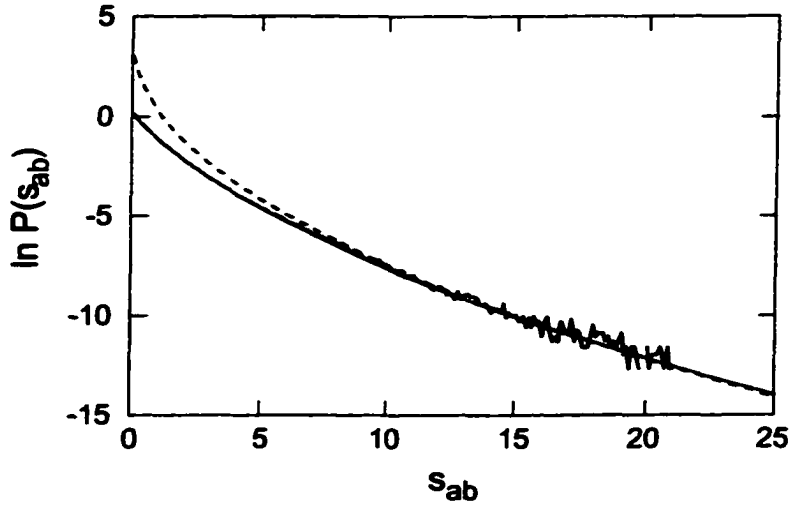

Figure 2.3: Comparison of experimental and theoretical results for sample b. The smooth solid curve represents the transform (Eq. 1.1) of the measured total transmission distribution b in Fig. 2.1. The short-dashed line gives the fit to the tail with the theoretical result, $P(s_{ab}) \sim \exp(-2\sqrt{g's_{ab}})$. The value of the fitting parameter, $g' = 3.20$, is close to the value, $g' = 3.06$, obtained from the total transmission measurement for the same sample. [From M. Stoytchev and A.Z. Genack, Opt. Lett. **24**, 262 (1999)]

$g' = 2/3var(s_a)$. The intensity distribution was also compared to the transform of the measured transmission distribution, given by Eq. 1.1. The transform for the sample b is shown as the smooth solid line in Fig. 2.2, which essentially overlaps with the measured distribution. These measurements, therefore, confirm that $P(s_{ab})$ has a stretched exponential tail to the power of 1/2 and is given by the transform of $P(s_a)$ of Eq. 1.1. Since, $var(s_a) = 2/3g$, for $L \ll \xi$, L_a, and because the localization threshold occurs at $g = 1$ in the absence of absorption, we make the conjecture that localization is achieved when $g' \sim 1$, or equivalently when $var(s_a) \sim 2/3$, whether absorption is present or not.

In strongly absorbing quasi-1D dielectric samples, $var(s_a)$ was found to increase sublinearly with length for diffusive waves [38]. This raised the possibility that the value of $var(s_a)$ might saturate with length and that absorption might introduce a

cut-off length for the growth of relative fluctuations. Here we show that, though the presence of absorption leads to a decrease in $var(s_a)$, this appropriately reflects a lessening of localization effects. The threshold for localization occurs at $g' \sim 1$, and for smaller values, g' falls exponentially with length.

We now consider the scaling of $var(s_a)$ in the polystyrene samples and its connection to localization. The role of absorption is investigated by comparing measurements to an analysis of the data that statistically eliminates the influence of absorption. Measurements are carried out in samples of loosely packed, 1.27-cm-diameter polystyrene spheres with a filling fraction of 0.52 within the frequency range 16.8-17.8 GHz. In these samples, $\ell \approx 5$ cm [102], giving $\xi \approx 5$ m for a tube diameter of 5 cm. The exponential attenuation length due to absorption is $L_a = 0.34 \pm 0.02$ m [38], and the diffusion extrapolation length, which gives an effective sample length for the statistics of transmission [103], $\tilde{L} = L + 2z_b$, is $z_b \approx 6$ cm [102]. For $L \ll \xi$, L_a, diffusion theory gives, $var(s_a) = 2\tilde{L}/3\xi$ [33, 34]. This result is shown as the horizontal short-dashed line in Fig. 2.3. As $g \rightarrow 1$ and localization threshold is approached, the scaling theory of localization suggests that g falls more rapidly [74], and hence $var(s_a)$ should increase superlinearly with sample length. Measurements of fluctuations in spectra of total transmission in ensembles of polystyrene samples give the results shown as the filled circles in Fig. 2.3. These results indicate that $var(s_a)$ increases sublinearly with length up to $L = 2$ m, which was the largest length at which accurate measurements of the total transmission were made.

To extend these studies of statistics in random waveguides to samples of greater lengths, we use Eq. 1.2. This allows us to relate the variance of the normalized total transmission to the variance of the normalized intensity, which is more readily measured in microwave experiments,

$$2var(s_a) = var(s_{ab}) - 1. \tag{2.3}$$

Transmitted field spectra are measured in ensembles of 2,000 polystyrene samples with use of a Hewlett-Packard 8772C network vector analyzer. The calculated intensity spectra yield $var(s_{ab})$ which gives the corresponding values of $var(s_a)$ using Eq. 2.3.

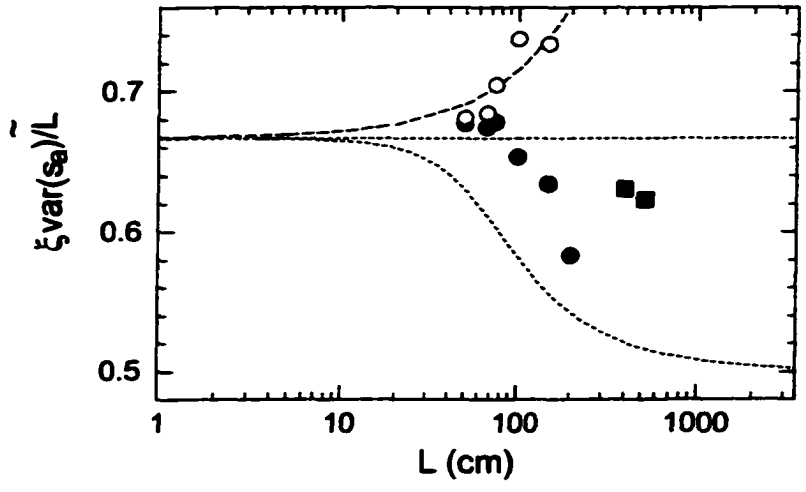

Figure 2.4: Influence of absorption and localization, separately and together, on $var(s_a)$ in random polystyrene samples. A semi-logarithmic plot of $\xi var(s_a)/\tilde{L}$ is presented to illustrate the measured scaling of $var(s_a)$ over a large range of L, as well as various theoretical predictions. The upper and lower short-dashed lines represent the two limits of diffusion theory: $L \ll \xi$, L_a and $L_a \ll L \ll \xi$, respectively. The filled circles are obtained from measurements of total transmission, while the filled squares are obtained from measurements of intensity. The circles are the results of an analysis that eliminates the affect of absorption, as explained in the text. The upper, long-dashed curve is a fit of these results to an expression incorporating the first-order localization correction to diffusion theory.

Values of $var(s_a)$ obtained in this way for $L \leq 2$ m agree within 3% with those shown as the filled circles in Fig. 2.4. The results for $L > 2$ m are shown in the figure as the squares. They indicate a more rapid, superlinear increase in $var(s_a)$ relative to the data for $L \leq 2$ m.

In these measurements, the effect of developing localization and absorption are intertwined. In order to obtain the values of $var(s_a)$ that would be measured in the absence of absorption, we use a procedure which is illustrated in Fig. 2.5. The measured field spectra are multiplied by the Fourier transform of a gaussian pulse in time to give the transmission spectra for this pulse. The spectrum is Fourier transformed to give the temporal response to a short incident gaussian pulse. To compensate for losses due to absorption, the time dependent field is multiplied by $\exp(t/2\tau_a)$, where t is the time delay from the incident pulse and $1/\tau_a$ is the absorption rate determined from measurements of the field correlation function with frequency shift [23]. Since the intensity is the square of the field, the decay rate of the field is a half of that of the intensity. The intensity of the modified field is shown as the short-dashed line in Fig. 2.5. This modified field is then transformed back to the frequency domain. Intensity spectra and the distribution and variance of intensity are then computed. The intensity distributions are in excellent agreement with calculations for diffusive waves [33, 34], which are described in terms of a single parameter g. The values of $var(s_a)$ found in this way are shown as the circles in Fig. 2.3. A fit of the leading order localization correction [42], $var(s_a) = 2\tilde{L}/3\xi + 4\tilde{L}^2/15\xi^2$, to the data gives the upper long-dashed curve in Fig. 2.4 with $\xi = 5.51 \pm 0.18$ m and $z_b = 5.25 \pm 0.31$ cm. These results are consistent with independent determination of these parameters [102]. The difference between the circles and the filled circles represents the amount by which $var(s_a)$ is reduced by absorption, and hence represents the extent to which absorption suppresses localization.

For diffusing waves, $var(s_a)$ was predicted to fall from $2\tilde{L}/3\xi$ for $L \ll L_a$ to $\tilde{L}/2\xi$ for $L \gg L_a$ [30, 117], following the lower short-dashed curve in Fig. 2.4. Notwithstanding the initial drop of $var(s_a)$ from $2\tilde{L}/3\xi$, our measurements rise above this curve as a result of enhanced intensity correlation, as $L \to \xi$. At $L = 5.2$ m, $var(s_a) = 0.6$, which is close to the critical value 2/3.

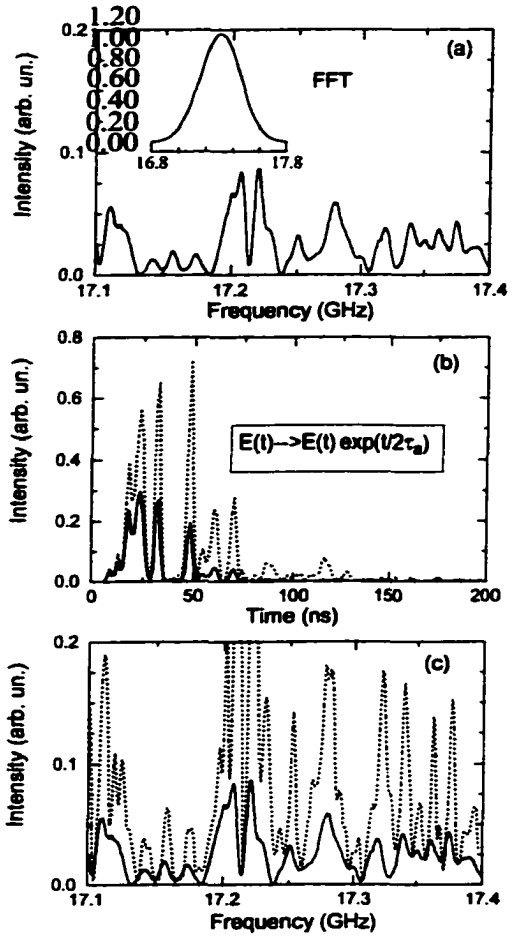

Figure 2.5: Statistical cancelation of absorption. (*a*) Intensity spectrum in a sample from the same ensemble as in Fig. 1.2. The field spectrum, from which the intensity spectrum is obtained, is multiplied by the spectrum of the pulse shown in the inset of (*a*) and Fourier transformed to the time domain. The result of the transform is squared to give the intensity pulse shown in (*b*) as the solid curve. The influence of absorption is removed in a statistical sense by multiplying field of the pulse by a factor $\exp(t/2\tau_a)$. The intensity of the modified pulse is shown as the short-dashed line in (*b*). The modified field is then Fourier transformed to the frequency domain. The field spectrum is then squared to give the transmitted intensity spectrum shown in (*c*) as the short-dashed curve and compared to the original spectrum. Intensity statistics computed using the transformed spectra are the same as predicted for a medium with the same real part of the dielectric function but without absorption.

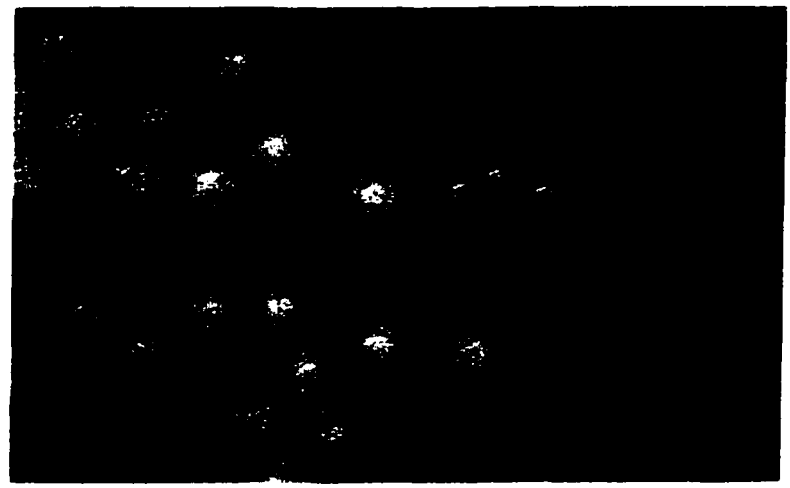

Figure 2.6: Alumina samples are composed of 0.95-cm-diameter alumina (Al_2O_3) spheres embedded in Styrofoam spheres. Styrofoam is nearly transparent for microwave and serves to control over alumina concentration. In this picture, Styrofoam spheres with diameter of 1.9 cm are shown. An inch ruler is also shown.

2.2 Strongly scattering quasi-1D dielectric samples

To study the statistics of transmission quantities for localized waves, we examine fluctuations of microwave intensity in strongly scattering samples of 0.95-cm-diameter alumina spheres (99.95% Al_2O_3). In order to have control over the alumina concentration, the alumina spheres are embedded in Styrofoam spheres of low refractive index (see Fig. 2.6). Measurements of intensity fluctuations are made in quasi-1D samples with an alumina volume fraction of $f = 0.068$ contained in a 7.3-cm-diameter copper tube. Large values of $var(s_a)$ indicate that the wave is localized in a narrow frequency window near the first Mie resonance of the alumina sphere for sample lengths $L > 60$ cm. A typical spectrum of the normalized transmitted intensity s_{ab} in the localization region for $L = 120$ cm is shown in Fig. 2.7. The sharp peaks in s_{ab} appear to be related to resonant transmission through localized photonic states in the sample. We expect that, when the frequency of the incident wave is tuned to resonance with localized states in the medium, transmission is appreciable. Between the peaks, transmission is exponentially small, so the incident wave is almost completely

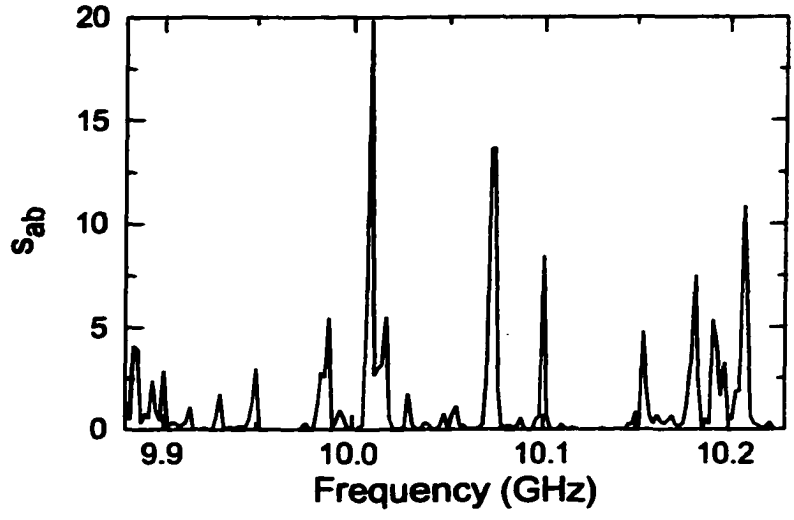

Figure 2.7: A typical spectrum of the normalized intensity s_{ab} near the first Mie resonance of the alumina spheres in a 80-cm-long alumina sample. The sharp and narrow line spectra and giant fluctuations shown have been predicted for localized waves and are unlike the corresponding spectra in diffusive samples as shown in Fig. 1.2.

reflected from the sample. The distribution function $P(s_{ab})$ calculated for an ensemble of 5,000 samples of $L = 120$ cm is shown in Fig. 2.8 and compared to the Rayleigh distribution. The measured distribution is remarkably broad with $var(s_{ab}) = 23.5$, and fluctuations greater than 300 times the average value are observed. The scaling of $var(s_a)$, determined using Eq. 2.3, at a number of frequencies near the first Mie resonance of the alumina spheres is shown in Fig. 2.9. We find that $var(s_a)$ increases exponentially once it becomes of order unity, as expected for a localization parameter. In the chapters that follow, we will discuss origins of localization in these alumina samples and will study the statistics of localized waves more closely.

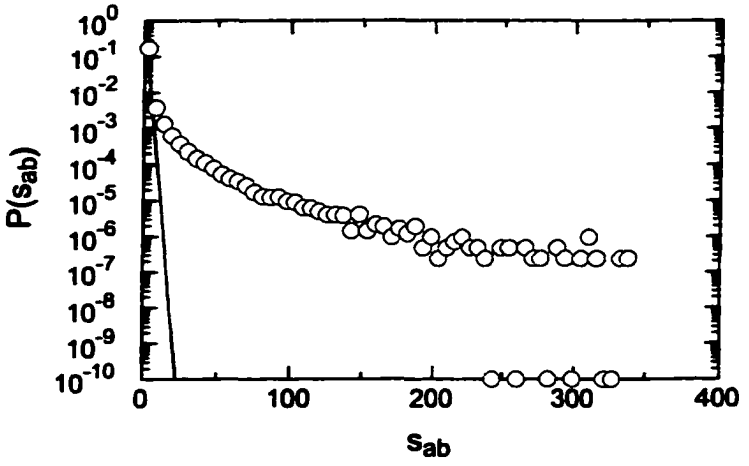

Figure 2.8: Semi-logarithmic plot of the distribution $P(s_{ab})$ for alumina samples with $L = 80$ cm. The distribution is obtained in an ensemble of 5,000 spectra within the frequency range 9.88-10.24 GHz, in which statistical parameters do not change substantially. The circles on the horizontal axis represent bins in which there is no measured intensity value. The solid line represents the Rayleigh distribution.

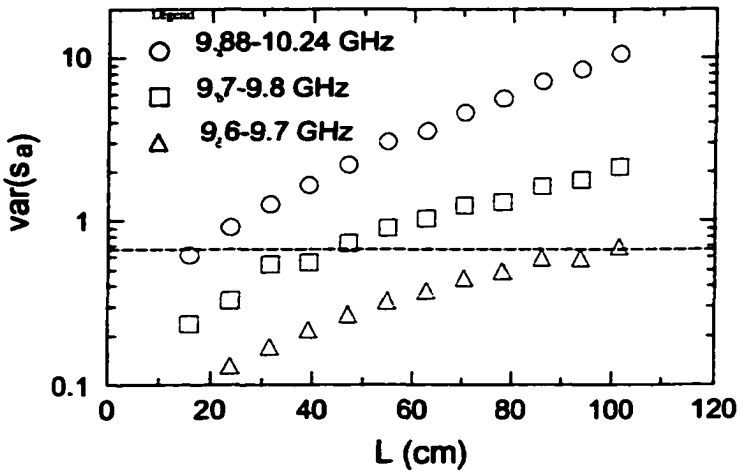

Figure 2.9: Scaling of $var(s_a)$ with L in alumina samples. The values of $var(s_a)$ averaged over the indicated frequency intervals are obtained using Eq. 2.3. Above a value of order unity, $var(s_a)$ increases exponentially. In the interval 9.88-10.24 GHz, $var(s_a) \sim \exp(L/L_{exp})$, with $L_{exp} \approx 42$ cm.

2.3 Periodic metallic wire mesh containing metallic scatterers

The availability of a measurable localization parameter makes it possible to determine the existence and the extent of localization in a variety of samples. This is illustrated in measurements of localization in periodic metallic wire meshes containing metallic scatterers. John [105] has proposed that photon localization could be achieved by introducing disorder in a periodic structure possessing a photonic band gap. These band gaps exist in the electromagnetic spectrum of a variety of periodic structures in analogy with the electronic band gaps in crystals [106]. In the photonic band gap, electromagnetic waves are evanescent. When disorder is introduced in such structures, localized states are created in the gap. The periodic structure that we examine is a simple cubic lattice made up of copper wires, with a lattice constant of 1 cm. The lattice has eight unit cells along each side and is enclosed in a section of a square waveguide. Measurements of microwave transmission in an empty wire mesh sample show a low-frequency gap with a cut-off frequency of 9.33 GHz (Fig. 2.10a) [107]. The network can be filled with 0.47-cm-diameter Teflon spheres in order to float various scatterers within the structure. The mean free path of randomly positioned Teflon spheres greatly exceeds the length of the structure, so that their only influence is to reduce the wavelength of radiation within the structure. The cut-off frequency of the Teflon-filled structure shifts to 7.58 GHz (Fig. 2.10b) [107]. When aluminum spheres with the same diameter replace some of the Teflon spheres, transmission peaks appear in the gap just below the band edge. As the scatterer density is increased, the gap fills in. Spectra of the average transmission measured in ensembles of 200 sample configurations at two aluminum sphere volume fractions, $f = 0.05$ and $f = 0.10$, are shown in Fig. 2.10c [107]. But such measurements leave open the question of whether the radiation is localized. To answer this question, we compute $var(s_a)$ for the two concentrations of aluminum spheres, whose frequency dependence is shown in Fig. 2.11. At $f = 0.05$, a window of localization is found, in which $var(s_a) \geq 2/3$. At twice this aluminum fraction, the smaller value of $var(s_a)$ indicates that the wave is extended. At this higher concentration, the density of states introduced by disorder

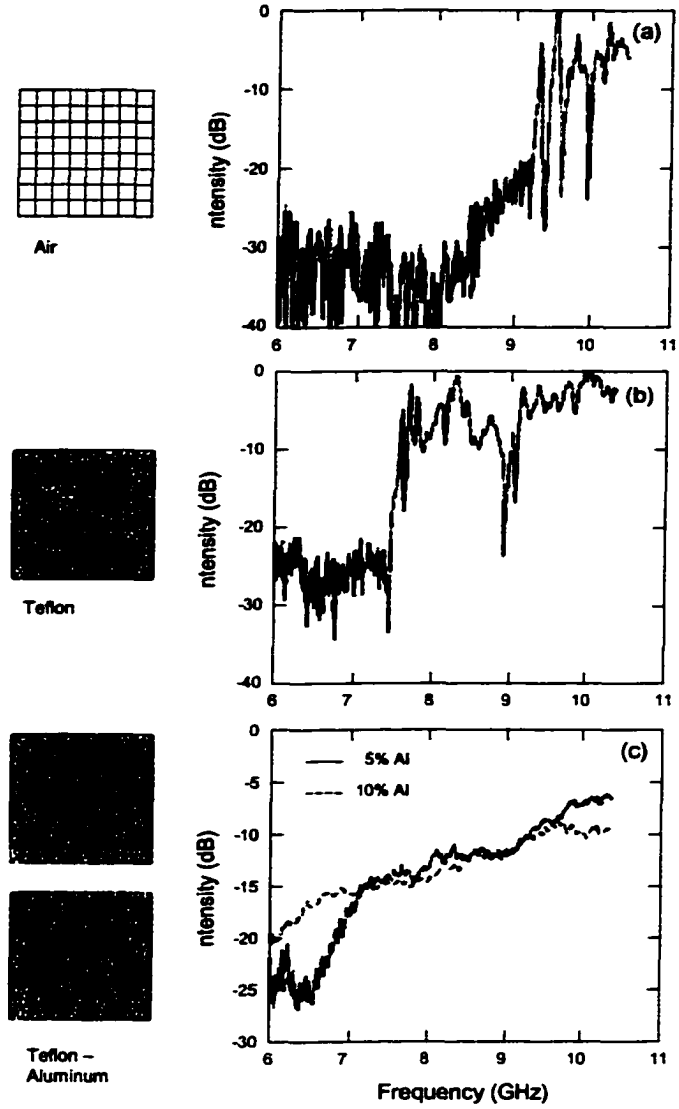

Figure 2.10: Schematic diagram of the wire mesh lattice filled with different media and associated transmission spectra. The structure has a lattice constant of 1 cm and is 8 unit cells on each side. In (a), the structure is in air. In (b), it is filled with Teflon spheres. In (c), the structure is filled with Teflon-aluminum mixtures at filling fractions of aluminum spheres of $f = 0.05$ and $f = 0.10$. The average transmission spectra obtained from 200 configurations for each value of f are shown. [From M. Stoytchev and A.Z. Genack, PRB **55**, R8617 (1997)]

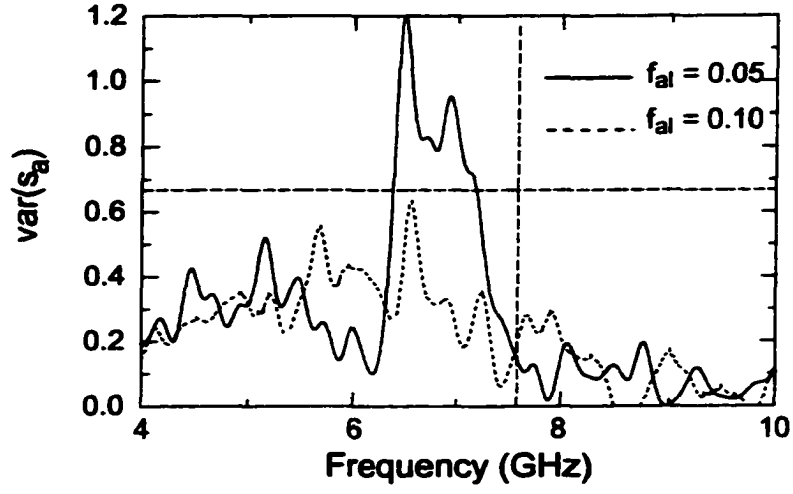

Figure 2.11: $Var(s_a)$ versus frequency in the metallic wire mesh containing aluminum scatterers. The broken vertical line indicates the position of the band edge in the periodic structure filled only with Teflon spheres. At an aluminum sphere volume fraction $f = 0.05$, $var(s_a)$ is markedly higher near the edge, rising above the localization threshold of 2/3 shown as the broken horizontal line. At $f = 0.10$, $var(s_a)$ is reduced and the wave is extended.

appears to be high enough that the wave is no longer localized. The gap is effectively washed out.

2.4 Three-dimensional samples of metallic scatterers

We have also used measurements of $var(s_a)$ to examine the claim that localization can be achieved in three-dimensional samples of metal spheres at various concentrations [91, 92, 108, 109]. We find that in samples of 0.47-cm-diameter aluminum spheres of length $L = 8.2$ cm and diameter $d = 7.5$ cm, with volume fraction of the aluminum spheres varied from 0.1 to 0.475, $var(s_a)$ never rises above the localization threshold of 2/3. A maximum value of 0.29 is reached at $f = 0.45$. Thus we conclude that three-dimensional localization is not achieved in these aluminum samples.

2.5 Conclusion

In conclusion, we have demonstrated that the variance of the normalized transmission is a robust localization parameter. It serves as a powerful tool in the search for and characterization of photon localization, even for absorbing samples. It has allowed us to locate regimes of localization in quasi-1D dielectric samples and in the periodic metallic wire lattice containing metallic scatterers, and to rule it out in three-dimensional collections of aluminum spheres. These results show that the statistics of transmission are essential aspects of localization.

CHAPTER 3
ORIGINS OF PHOTON LOCALIZATION IN RESONANT MEDIA

Photon localization has been of intense interest since it was first proposed as the analog of electron localization [76]. Accurate measurements of the statistics of the electromagnetic field and intensity and of the total transmission in random samples have deepened our understanding of mesoscopic physics and localization. However, the very possibility of photon localization in three-dimensional systems without substantial crystalline order has been called into question by the barriers to achieving and detecting electromagnetic localization. Unlike electrons that can be trapped by the Coulomb interaction at atomic sites, photons are not bound by individual particles. They are not strongly scattered by particles either, except at Mie resonances where the scattering cross section can considerably exceed the geometric cross section. To preserve the strength of scattering, however, particles must be separated by at least the diameter of the scattering cross section, requiring particle separation that are larger than the wavelength λ. It would then appear that the Ioffe-Regel-like condition for localization in three dimensions [81], $\ell_{sc} \leq \lambda/2\pi$, where ℓ_{sc} is the scattering mean free path, cannot be satisfied by collections of independent resonant scatterers [110]. Measurements of exponential scaling of transmission [92, 93, 96] have not definitively established localization because the possible presence of absorption could also lead to exponential decay of intensity within a sample. However, recent measurements of coherent backscattering in macroporous GaP networks [111] along with theoretical predictions of [97] suggest that the approach to localization can be observed in the rounded backscattering peak from weakly absorbing samples. Besides, the variance of relative fluctuations has been shown to provide a decisive test for localization, even in the presence of strong absorption [44]. This provides a sure guide in the search for localization and raises the possibility that measurements of

key scattering parameters can be used to sort out the precise material and structural characteristics that may edge samples towards and potentially across the localization threshold.

In this chapter, we present microwave measurements of the frequency variation of three key localization parameters in quasi-1D samples composed of randomly positioned alumina spheres in an open copper tube. These are the Thouless number [73], which is the ratio of the width to the spacing between quasistates of a random medium, $\delta = \delta\nu/\Delta\nu$, the dimensionless conductance g [74], and a parameter g' [44], which represents the inverse of the variance of transmission normalized to its ensemble average value. These parameters capture, respectively, the relation to localization of average dynamics, average static transmission, and static fluctuations. Their measurement makes it possible to identify a narrow window of localization above the first Mie resonance and to probe a constellation of factors that foster localization, including size, concentration, and structural correlation.

We present the first direct measurement of the Thouless number. The Thouless criterion identifies the onset of localization as the point at which the level width $\delta\nu$ becomes smaller than the level spacing $\Delta\nu$ [73]. Beyond this point, transport is inhibited since modes in different blocks of a sample do not overlap. The level width $\delta\nu$ is identified with the field correlation frequency [72]. This is inversely related to the width of the time-of-flight distribution of the transmitted wave and to the average transit time through the medium, τ [45]. The level spacing $\Delta\nu$ is the inverse of the density of states, $\Delta\nu = 1/N(\nu)$, thus giving $\delta = \delta\nu N(\nu)$. The hurdles to localizing radiation, even in resonant media, can be seen from a dynamical perspective. The precipitous drop in $\delta\nu$ expected at resonance, reflecting the sharp peak in τ, does not necessarily result in a diminished value of δ because it is countered by an increasing value of $N(\nu)$.

The dimensionless conductance g can be obtained in electronic systems from the measurement of the conductance $G = (e^2/h)g$, whereas for classical waves it can be found from the measurement of the total transmission T_a, since $g = N\langle T_a\rangle$, where $N = Ak^2/2\pi$ is the number of transverse modes of a sample. For diffusive waves in nonabsorbing samples of length L, $g = N\ell/L$. Thus the parameter g is essentially the

number of diffusing channels in a sample, and so the localization threshold is reached when its value falls below unity [112]. This is consistent with the Thouless criterion for localization, since for diffusive waves, $g = \delta > 1$ [74].

In the diffusive limit and in the absence of absorption, the variance of the total transmission normalized to its ensemble average is given by $var(s_a) = 2/3g$ [34, 38, 42]. The measure of fluctuations, $g' = 2/3var(s_a)$, thus reduces to g in the above limit. The localization transition occurs when $g' \sim 1$ [44]. Since $var(s_a)$ and $var(s_{ab})$ are related by $var(s_a) = \frac{1}{2}(var(s_{ab}) - 1)$ [34, 44], we are able to evaluate g' either from measurements of total transmission, using an integrating sphere [38], or from local measurements of intensity [44].

Measurements of field transmission spectra are carried out in low-density collections of 0.95-cm-diameter alumina spheres (99.95% Al_2O_3) with use of a Hewlett-Packard 8772C network vector analyzer. Low densities are produced by embedding the alumina spheres in Styrofoam spheres of low refractive index. The index of refraction n of the alumina spheres is inferred from a comparison of the measured extinction coefficient of the coherent intensity I_c in three-dimensional samples with an alumina volume fraction $f = 0.010$ with the calculated scattering cross section σ_{sc} for isolated alumina spheres. In the independent-scattering approximation, $\ln I_c = -n_{sc}\sigma_{sc}L$, where n_{sc} is the number density of the alumina scatterers. The natural logarithm of I_c is compared to calculations of σ_{sc} with $n = 3.14$ in Fig. 3.1. This gives the closest correspondence between the positions of the Mie resonances and those of the dips in $\ln I_c$.

Measurements of microwave propagation and localization are made in quasi-1D samples with an alumina volume fraction of $f = 0.068$ contained in a 7.3-cm-diameter copper tube at $L = 80$ cm and $L = 12$ cm. The alumina spheres are put at centers of 1.9-cm-diameter Styrofoam spheres. An ensemble of 5,000 statistically equivalent random samples is created by rotating the tube between successive field measurements. The incident mode a is parallel to the sample axis. The outgoing field is detected at a point on the output surface of the sample. For each sample configuration, the field spectrum yields the corresponding frequency variation of the transmitted intensity I_{ab}. The ensemble average intensity $\langle I_{ab} \rangle$ for $L = 80$ cm samples shown in Fig. 3.2a

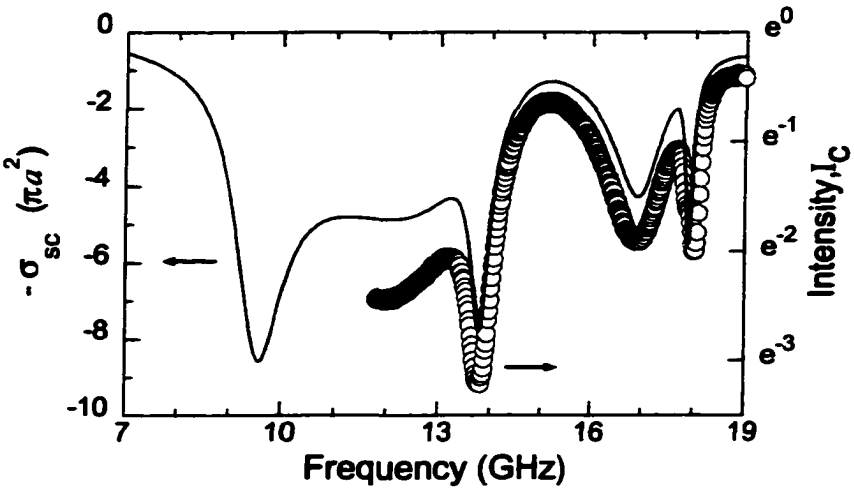

Figure 3.1: Comparison of the scattering cross-section σ_{sc} of a 0.95-cm-diameter alumina sphere (solid) and the extinction of the coherent intensity I_c in a 3D alumina sample with $f = 0.010$ (circles). In calculations, the alumina sphere is assumed to be lossless and the refractive index is adjusted so that the positions of the Mie resonances are located at the dips in the experimental data. The curve shown is for $n = 3.14$.

exhibits distinct dips near each of the Mie resonances. The resonant character of scattering is further indicated by the sharp peaks in the spectrum of the average photon dwell time, seen in Fig. 3.2b. The transit time is given by $\tau = \langle s_{ab} d\phi_{ab}/d\omega \rangle$, where ϕ_{ab} is the phase of the field and ω is the angular frequency [58]. Since low transmission can be due to absorption and long dwell time can be associated with microstructure resonances, these indicators do not provide a definitive measure of the closeness to the localization threshold. This can be obtained, however, from the measurement of $var(s_{ab})$ shown in Fig. 3.2c. For diffusive waves obeying Rayleigh statistics, $var(s_{ab}) = 1$. Lower values below 8.5 GHz indicate a significant ballistic component in the transmitted field, while higher values indicate the presence of substantial long-range correlation. The horizontal dashed line in Fig. 3.2c represents the localization threshold, $var(s_{ab}) = 7/3$, which corresponds to $var(s_a) = 2/3$ or, equivalently, to $g' = 1$. The localization threshold in this quasi-1D sample is crossed in a narrow frequency range above the first Mie resonance. Large fluctuations in

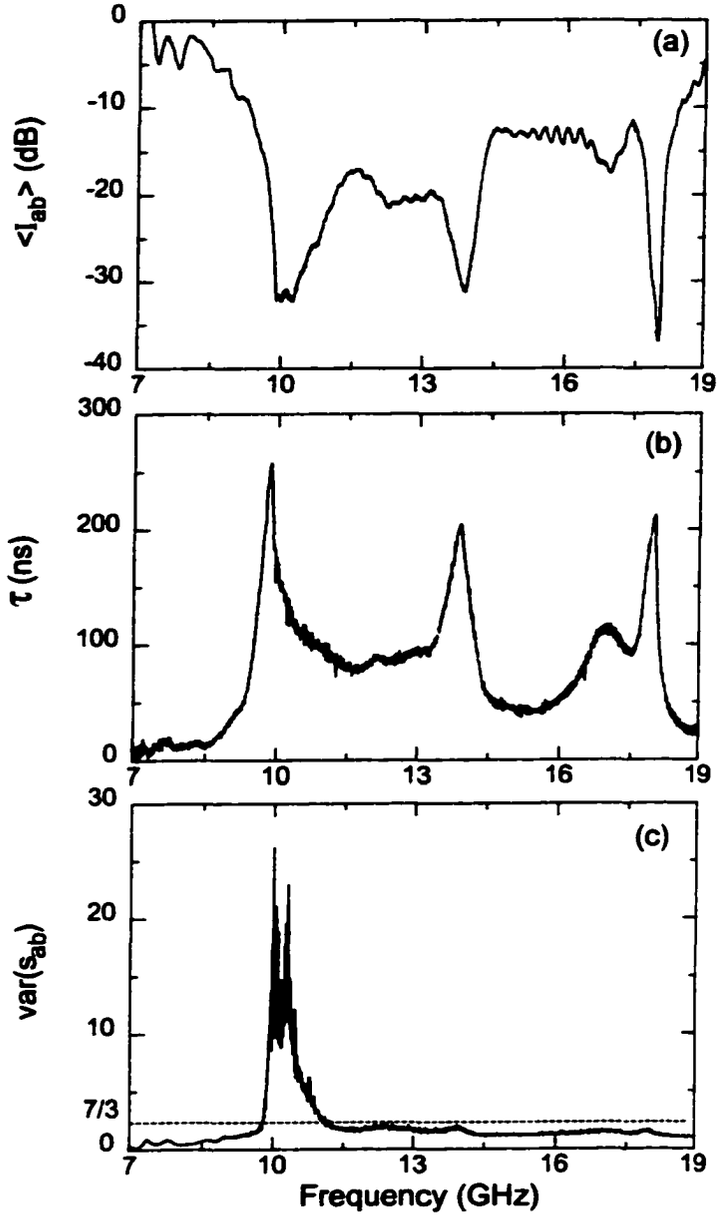

Figure 3.2: (a) Average transmitted intensity $\langle I_{ab} \rangle$, (b) average photon dwell time τ, and (c) $var(s_{ab})$ in a quasi-1D alumina sample of $L = 80$ cm and $f = 0.068$. The dashed line is the localization threshold, $var(s_{ab}) = 7/3$.

measurements of $var(s_{ab})$ above the localization threshold, seen in Fig. 3.2c, are a result of the greatly enhanced tail of the intensity distribution for localized radiation, seen in Fig. 2.8.

In order to take a closer look at the localization region, the data in Fig. 3.2 are superimposed and displayed using an expanded scale in Fig. 3.3a. The shift of

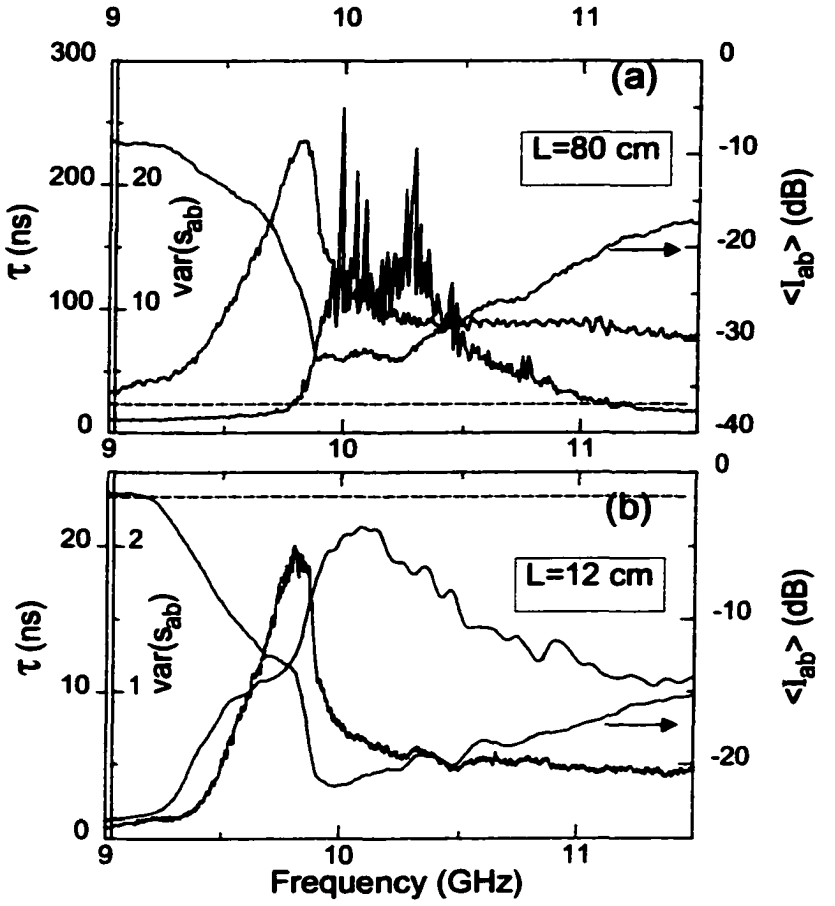

Figure 3.3: $\langle I_{ab} \rangle$, τ and $var(s_{ab})$ superimposed over the frequency range of the first Mie resonance: (a) $L = 80$ cm, (b) $L = 12$ cm. The dashed line is the localization threshold, $var(s_{ab}) = 7/3$.

extrema in $\langle I_{ab} \rangle$ and in $var(s_{ab})$ to frequencies above the maximum in τ indicates that localization occurs above the resonant peak. Since localization occurs within a trough

of δ in a frequency range in which τ is smaller than its peak value by a factor of three, $N(\nu)$ must drop from its peak value on resonance by an even greater factor. We also expect that in the absence of absorption, $g' \simeq g$, and that the peak in $var(s_{ab})$ should occur at the same frequency as the dip in $\langle I_{ab} \rangle$ rather than at higher frequency as seen in Fig. 3.3a. The shift observed in the corresponding spectra in Fig. 3.3a is principally a result of the peak in photon dwell time, which increases absorption and suppresses $\langle I_{ab} \rangle$ more than $var(s_{ab})$ at the resonance. Enhanced absorption on resonance is also the cause of the drops in transmission at higher Mie resonances in Fig. 3.3a.

To investigate the factors that incline a sample towards localization, we carry out the measurements presented in Fig. 3.3a in a shorter sample of $L = 12$ cm (see Fig. 3.3b), so that $\ell < L < \xi, L_a$, where $\xi = N\ell$ is the localization length and L_a is the exponential absorption length. In this weakly absorbing sample, we find that transport is diffusive above 9.6 GHz, where $1 < var(s_{ab}) < 7/3$ (Fig. 3.3b), so that g, g', and δ can be associated unambiguously with the proximity to the localization threshold. The quantities g and g' are obtained from measurements of the total transmission T_a, via expressions $g = N\langle T_a \rangle$ and $g' = 2/3var(s_a)$. Good agreement between g and g' is found, as seen in Fig. 3.4. Also notice that, since the minimum of g occurs above the resonance, the minimum of ℓ must also lie above that of ℓ_{sc}.

To examine more closely the balance of competing effects near the resonance, we measure $\delta\nu$, $\Delta\nu$, and δ. The level width $\delta\nu$ is determined from measurements of the field correlation function with frequency shift. We find that $\delta\nu$ shown in Fig. 3.5b is related to the average diffusion time in Fig. 3.3b, $\tau = L^2/6D = 1/6\delta\nu$. The level spacing $\Delta\nu$ is found by measuring transmission between two probes in the tube with copper end caps. In this case, line widths are narrowed and mode spacing can be measured (see Fig. 3.5a). When determining $\Delta\nu$ both positive and negative peaks in spectra of $d\phi_{ab}/d\omega$ are accounted. The negative peaks appear because of interference between two closely spaced modes. A comparison of $\Delta\nu$ calculated for an ensemble of 360 sample configurations and $\delta\nu$ is shown in Fig. 3.5b. We find that, whereas $\delta\nu$ and $\Delta\nu$ attain their minimum values at the resonance, their ratio is a minimum above the resonance. In the trough of δ, where the measurements of $\Delta\nu$ are most reliable by virtue of the lowest values of $N(\nu)$, δ is in a good agreement with g and

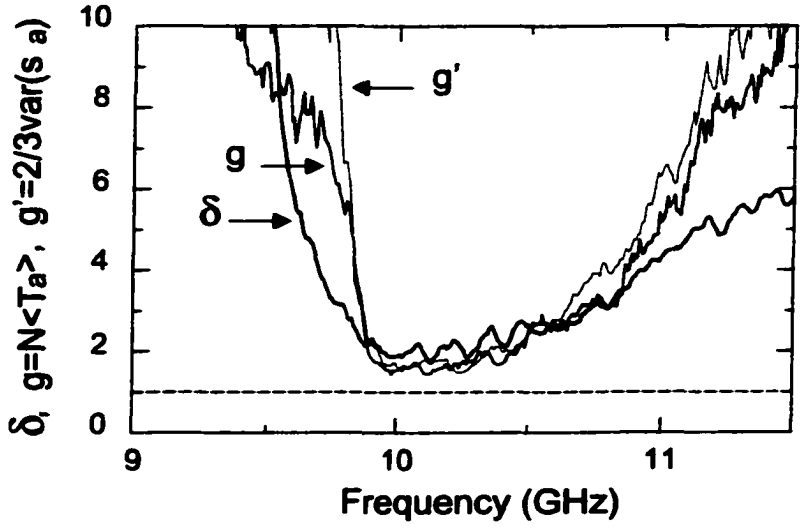

Figure 3.4: Localization parameters δ, g and g' over the frequency range of the first Mie resonance in an alumina sample of $L = 12$ cm. The dashed line is the localization threshold.

g' (Fig. 3.4).

The increase above resonance in $\Delta\nu$, obtained from a calculation of $N(\nu)$ in the independent-scattering approximation [81], is well below the measured increase (see Fig. 3.5b). This suggests that increasing the density of resonant scatterers beyond the point at which they begin to interact suppresses the density of states and thereby fosters localization. A decrease in $N(\nu)$, on the other hand, was predicted by John [105] for nearly periodic samples. Indeed, for periodic samples exhibiting a complete photonic band gap, the vanishing of $N(\nu)$ automatically results in localization within a pseudogap, when disorder is introduced. We find that, when the alumina spheres are displaced by half of their radius from the centers of the embedding Styrofoam spheres, $var(s_{ab})$ is only slightly suppressed. For a $L = 55$ cm alumina sample, $var(s_{ab})$ drops from 6.0 to 4.5 at its maximum. This small reduction, for a considerable broadening of the radial correlation function, suggests that collective scattering from randomly positioned alumina spheres itself and not only their residual positional order is the

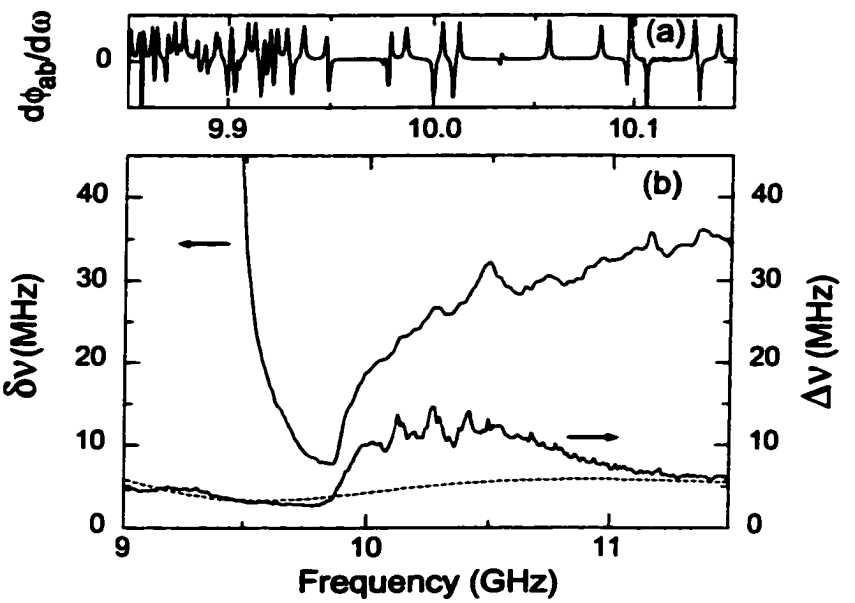

Figure 3.5: (a) Part of a spectrum of $d\phi_{ab}/d\omega$ for a single configuration with the peaks marking the mode frequencies and (b) the level width $\delta\nu$ and the average level spacing $\Delta\nu$ in a $L = 12$ cm alumina sample. At all frequencies, $\delta\nu > \Delta\nu$. The dashed line is the inverse of $N(\nu) = (8\pi\nu^2/v_0^3)(v_p/v_E)V$ [81], where v_p and v_E are the phase [81] and the energy [80] velocity, respectively, v_0 is speed of light in the effective medium, and V is the sample volume.

chief reason for the sharp drop in $N(\nu)$ above the first Mie resonance.

In conclusion, we have measured the dimensionless conductance, the variance of transmission fluctuations, and the Thouless number in low-density collections of alumina spheres in a quasi-1D geometry. We find these are equivalent measures of localization for $L < L_a, \xi$. For samples longer than L_a, only $var(s_a)$ serves as a reliable guide to localization, which is found in a narrow frequency range above the first Mie resonance in the longer sample. Localization does not occur on resonance because the narrowing of the level width is offset by the enhancement of the density of states. However, a sharp drop in $N(\nu)$ above resonance leads to a minimum in δ. The drop in $N(\nu)$ and the consequent appearance of localization are the result of collective scattering.

CHAPTER 4
STEADY-STATE TRANSMISSION OF LOCALIZED WAVES

Measurements of the transmitted microwave field in ensembles of alumina samples allow us to study the changing character of both static and dynamic aspects of transport in the transition from diffusive propagation to localization. In this chapter, we focus on the statistics of transmitted intensity, which is a steady-state property. The statistics of wave dynamics is considered in the next chapter, which treats distributions of quantities related to spectral derivatives of the phase.

4.1 Resonant transmission of localized waves

Transport of localized waves in bounded samples is completely different from that of extended waves. For most frequencies, transmission through a localized sample of length L is a result of evanescent coupling of the incident wave to the outer boundary, $T \sim \exp(-L/\xi)$. However, when the frequency of the incident wave is tuned into resonance with a localized state in the sample, the wave couples to the boundary through the localized state. In this case, the corresponding transmission is $T \sim \exp(-2\Delta/\xi)$, where Δ is the distance from the center of the localized mode to the middle of the sample [113], which is exponentially greater than the transmission at a typical frequency. This results in giant fluctuations in a resistance with voltage [114, 115, 116] and in microwave transmission with the frequency of the incident wave [44]. The width of the resonant transmission line is inversely proportional to the lifetime τ, which gives the rate at which the wave is dissipated due to leakage and absorption in the medium. Since the spectral density of localized states in the sample is ordinarily large, and because the localized states in the spectrum tend to be closer to each other [79], the isolated transmission lines are difficult to observe. In this regard, the

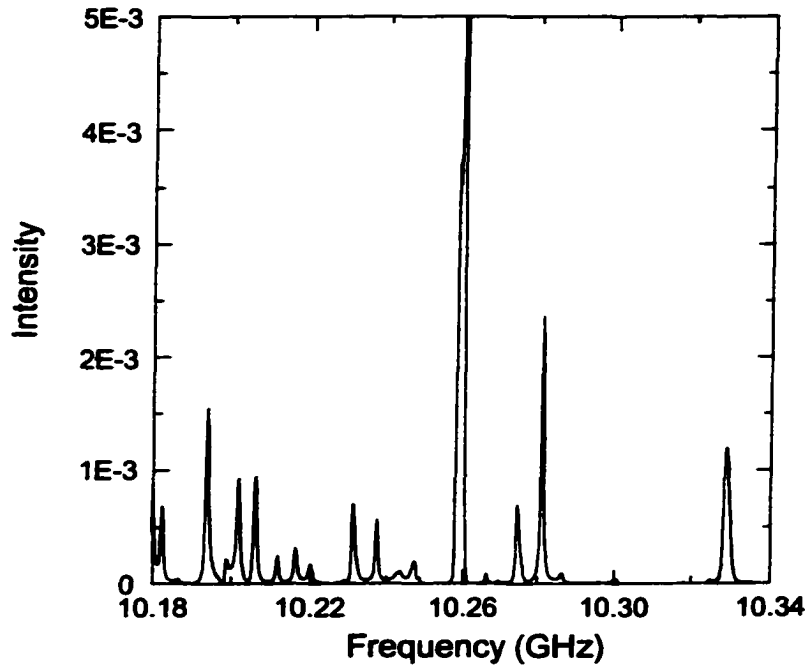

Figure 4.1: Frequency dependence of microwave intensity within the localization window, in a $L = 120$ cm alumina sample with the alumina volume fraction $f = 0.073$ and cooled to 77 K. The sharp peaks in the intensity spectrum represent resonant transmission through single localized states.

spectral peaks in Fig. 2.7 are, for the most part, the result of microwave transmission through a number of localized states. In order to observe isolated lines in transmission spectra through alumina samples, we increase the density of alumina spheres in the copper tube from $f = 0.068$ to 0.073 and cool off the tube with liquid nitrogen. The first leads to a higher residual order in the sample and to a decrease of the density of states in the localization window. The second significantly decreases absorption, and thus decreases the spectral width of the states. A spectrum of transmitted microwave intensity within the localization window, in a cooled alumina sample of length $L = 120$ cm, is shown in Fig. 4.1. A number of isolated transmission lines can be seen, though a number of lines still overlap. A part of this spectrum is displayed in Figs. 4.2 and 4.3 at higher resolution. In Fig. 4.2, a roll-up of the phase of the

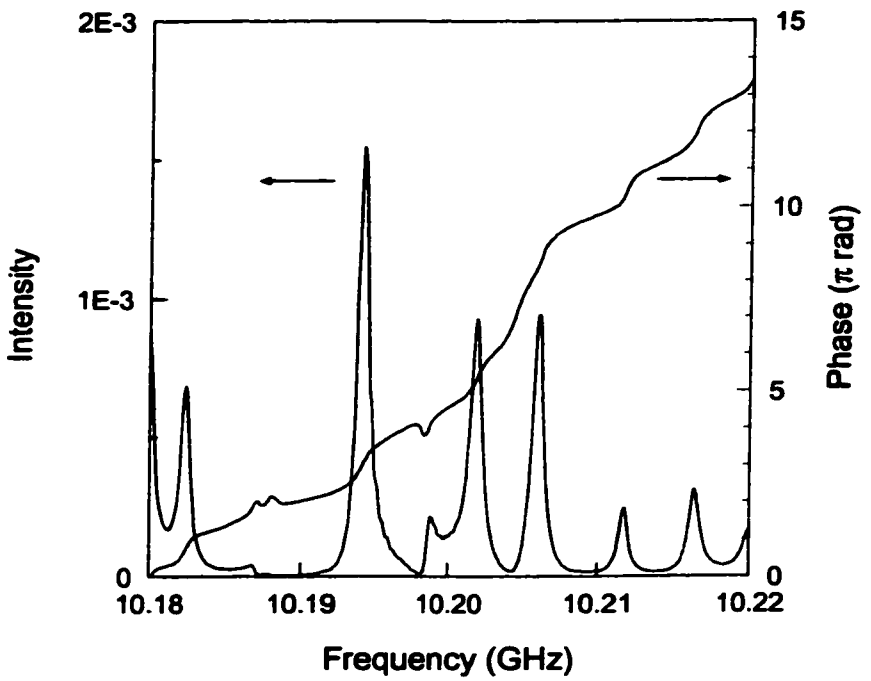

Figure 4.2: Intensity and phase of localized waves in a cooled alumina sample with the length $L = 120$ cm and alumina volume fraction $f = 0.073$. The phase jumps by π, as the frequency is swept through intensity peaks, indicating the resonant nature of localized wave transmission.

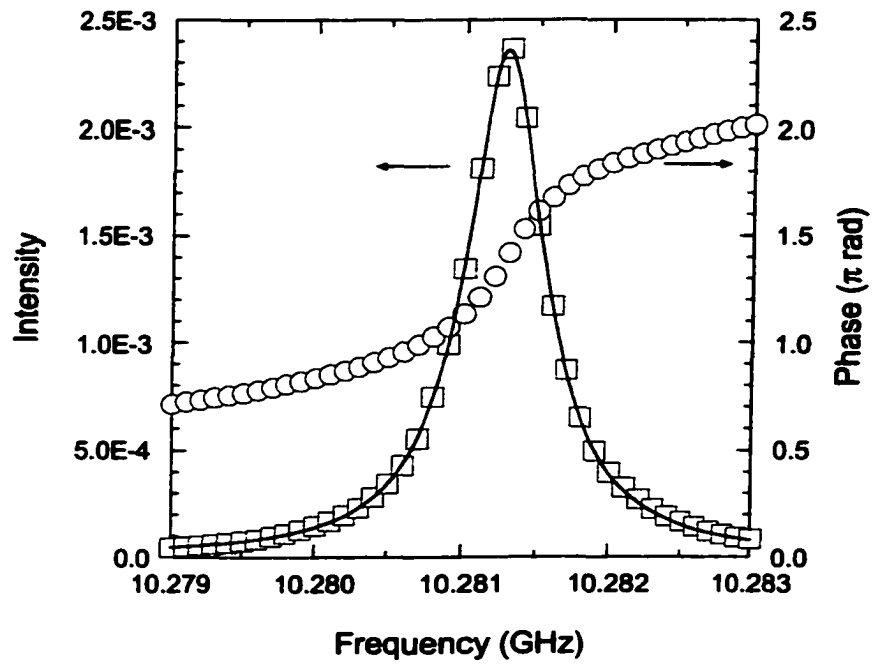

Figure 4.3: Isolated resonant transmission line in the localized wave spectrum. The transmitted intensity and the phase are shown by squares and circles, respectively. The solid line is the fit of Lorentzian form to the intensity data, which gives the line width, $b = 0.64$ MHz.

transmitted field as the frequency is swept through the frequency interval is shown as well. For most transmission lines, the phase is seen to jump by π, as the frequency is swept through the peak in intensity, indicating the resonant nature of propagation. Near resonance, the intensity has a Lorentzian form, $I(\nu) = a(b/2)^2/((\nu - \nu_0)^2 + b^2)$, where a is the height of the intensity peak, b is the total width at half-maximum, and ν_0 is the central frequency. The isolated resonant transmission line, which is just above $\nu = 10.28$ GHz in the spectrum in Figs. 4.1, is shown in Figs. 4.3 with a minimum frequency step of 0.1 MHz. The measured intensity and phase are shown by squares and circles, respectively. A Lorentzian fit to the intensity data is shown as the solid line and gives $a = 2.36$E-3, $b = 0.64$ MHz, and $\nu_0 = 10.2813$ GHz. This allows estimating the time that the wave spends on resonance in the cooled sample, $\tau = 1/b = 1.54$ μs.

Besides demonstrating the resonant nature of wave propagation in localized media, the microwave field measurements in cooled alumina samples give important clues regarding the statistics of localized waves. In particular, the sharp peaks associated with resonant propagation should result in broadened distributions of transmitted quantities. In addition, the joint resonant behavior of the wave intensity and phase leads to a new type of correlation between the intensity and delay time. This is associated with a profound change in the statistics of dynamics of localized waves as compared to those of extended waves.

4.2 Scaling of transmitted intensity for diffusing and localized waves

The key result of Chapter 2 was the demonstration that the variance of the normalized tranmission is a proper localization parameter which accurately reflects the extent of localization, even in the presence of absorption. At a threshold value of order unity, $var(s_a)$ crosses over from a nearly linear scaling for extended waves to exponential scaling for localized waves (see Fig. 2.9). Since the universal scaling of g is an essential characteristic of localization in the absence of absorption [74, 98], it is interesting to examine the scaling of transmission in the presence of absorption.

Measurements of local intensity were carried out in lossy samples of alumina spheres contained in the copper tube at an alumina volume fraction $f = 0.068$ and with sample lengths from $L = 30$ to 105 cm. The scaling of $var(s_a)$ in Fig. 2.9 suggests that the wave is localized in these samples for sample lengths in excess of 60 cm in a narrow frequency range centered at $f \approx 10$ GHz, slightly above the first Mie resonance of the alumina spheres. Outside this range, the wave is extended even in the longest samples with $L = 105$ cm. Here we compare the scaling of the transmitted intensity in the frequency interval of 9.94-10.1 GHz, within the window of localization, to that for diffusing waves in the interval of 17.95-18.05 GHz near the fifth Mie resonance of the alumina spheres. These frequency intervals are sufficiently narrow that within them propagation parameters are nearly constant.

The logarithm of the ensemble average of transmitted intensity, $\ln\langle I_{ab}\rangle$, and the ensemble average of the logarithm of intensity, $\langle \ln I_{ab}\rangle$, in the lower and upper frequency interval, are shown in Fig. 4.4a and Fig. 4.4b, respectively. In the upper frequency interval, $\ln\langle I_{ab}\rangle$ and $\langle \ln I_{ab}\rangle$ decrease linearly with sample length (Fig. 4.4b). The corresponding attenuation lengths, ℓ_1 and ℓ_2, are found from a linear fit to be the same, within the accuracy of the experiment, $\ell_1 \approx \ell_2 \approx 10.1$ cm. The fact that the average intensity, $\langle I_{ab}\rangle \propto \exp(-L/\ell_1)$, and the so-called typical intensity, $\exp\langle \ln I_{ab}\rangle \propto \exp(-L/\ell_2)$, decay with the same attenuation length suggests that, for $L > L_a$, the n-th moment of the intensity distribution for diffusing waves is multiplied by $\exp(-nL/L_a)$, $\langle I^n\rangle \sim \exp(-nL/L_a)$, as a result of absorption. In this case, the statistics of the intensity normalized by its ensemble average value is essentially the same as in nonabsorbing samples. This may explain, in particular, that the variance of the normalized intensity accurately reflects the extent of localization in absorbing samples [44].

The problem of transmission through a many-channel random waveguide with absorption was treated by Brouwer [117], in the limit $\xi \gg L_a$. It was shown, in particular, that in the localization limit $L \gg \xi$, $\ln\langle I_{ab}\rangle \propto -L/2\xi - L/L_a$ and $\langle \ln I_{ab}\rangle \propto -3L/4\xi - L/L_a$. In Fig. 4.4a, $\ln\langle I_{ab}\rangle$ and $\langle \ln I_{ab}\rangle$ decrease linearly with L, with the corresponding attenuation lengths $\ell_1 \approx 18.0$ cm and $\ell_2 \approx 12.6$ cm. These are, however, inconsistent with the results of [117]. Furthermore, [117] predicts the

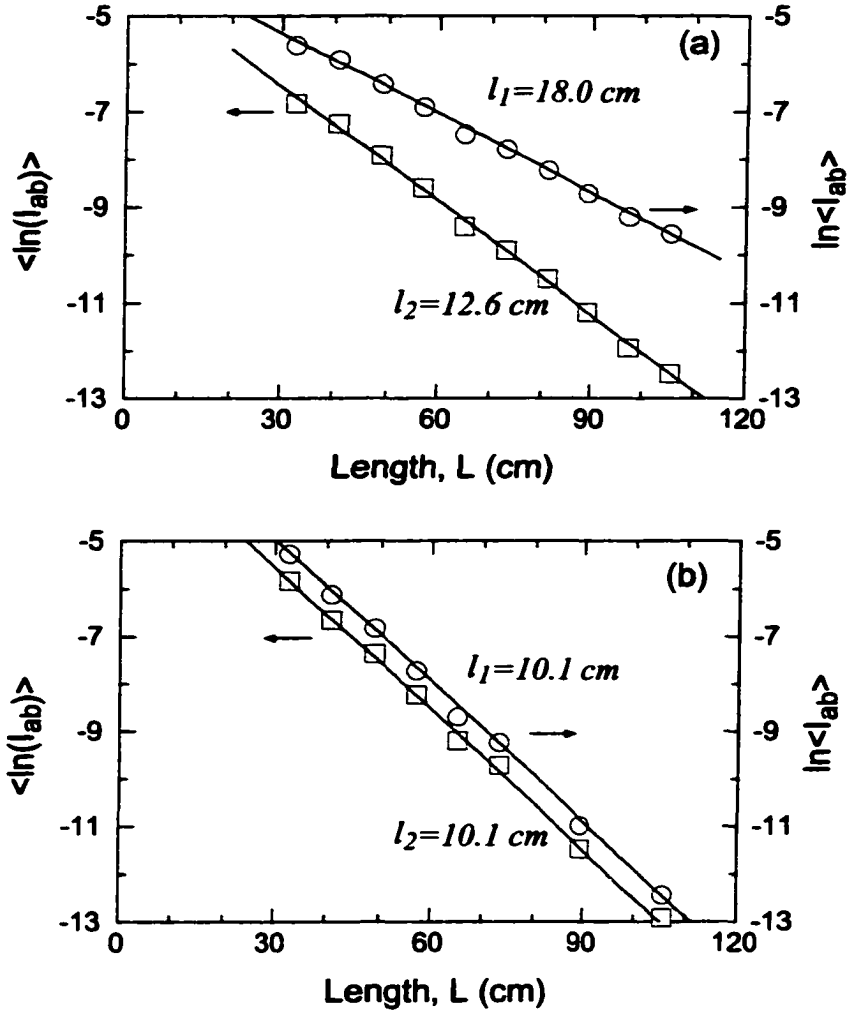

Figure 4.4: Scaling with sample length of the logarithm of the average intensity, $\ln\langle I_{ab}\rangle$, (circles) and of the ensemble average of the logarithm of intensity, $\langle \ln I_{ab}\rangle$, (squares) in the alumina samples, in the frequency intervals (a) 9.94-10.10 GHz and (b) 17.95-18.05 GHz. The solid lines are a linear fit to the experimental data with ℓ_1 and ℓ_2, the corresponding attenuation lengths for $\ln\langle I_{ab}\rangle$ and $\langle \ln I_{ab}\rangle$.

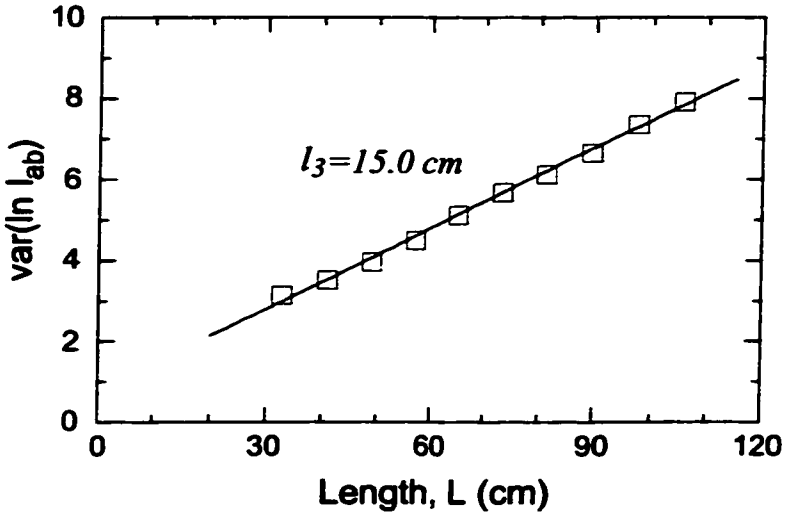

Figure 4.5: Scaling with sample length of $var(\ln I_{ab})$ (squares) in the alumina samples, in the frequency interval 9.94-10.10 GHz. The solid line is a linear fit to the experimental data, and $\ell_3 \approx 15.0$ cm is the corresponding characteristic length.

following behavior for $var(\ln I_{ab})$, $var(\ln I_{ab}) \propto L/2\xi$. In the lower frequency interval, $var(\ln I_{ab})$ increases linearly with sample length L (Fig. 4.5). A linear fit to the experimental data gives the characteristic length, $\ell_3 = 1/2\xi \approx 15.0$ cm. This gives $\xi \approx 7.5$ cm, which is clearly well below the localization length in these samples.

In contrast, a realistic value for ξ can be obtained from the scaling for localized waves of the variance of $\ln I_{ab}$ for a waveguide without absorption, $var(\ln I_{ab}) \propto 4L/\xi$ [118], assuming that this scaling does not change in the presence of absorption. This is consistent with the results for diffusing waves in the upper frequency interval (Fig. 4.4b), which suggest that scaling of the central moments, or cumulants, of the distribution of $\ln I_{ab}$ is not affected by absorption. Should this be the case, the characteristic length ℓ_3 is then $\ell_3 = 4/\xi$, giving $\xi \approx 60.0$ cm, which is the same estimate for ξ, as obtained from the analysis of $var(s_a)$ in Fig. 2.9.

In the absence of inelastic precesses, in the localization limit $L \gg \xi$, the average transmittance decays as, $\langle T \rangle \propto \exp(-L/2\xi)$, whereas the typical transmittance decays as, $\exp\langle \ln T \rangle \propto \exp(-2L/\xi)$ [118]. The same is true for all transmission

quantities, since for large L, the transmittance T is dominated by transmission in the mode with the largest ξ. We then assume in the presence of absorption, $\langle I_{ab} \rangle$ and $\exp\langle \ln I_{ab} \rangle$ are multiplied by $\exp(-L/L_a)$, which gives the following attenuation lengths, $\ell_1 = -1/2\xi - 1/L_a$ and $\ell_2 = -2/\xi - 1/L_a$, which differ from the corresponding equations of [117], but are consistent with the scaling of diffusive waves in the upper frequency interval (Fig. 4.4b). Solving for ξ and L_a, we obtain $\xi \approx 63.0$ cm and $L_a \approx 21.0$ cm, in the lower frequency interval. This estimate for ξ is in agreement with those obtained from the scaling of $var(\ln I_{ab})$ and of $var(s_a)$. However, as the proposed scaling for $\langle I_{ab} \rangle$ and $\exp\langle \ln I_{ab} \rangle$ is valid in the localization limit $L \gg \xi, L_a$, the values of ℓ_1 and ℓ_2 apply for the full range of L. In other words, the localization threshold does not show up in the scaling of $\ln\langle I_{ab} \rangle$ and $\langle \ln I_{ab} \rangle$ in Fig. 4.4a. This may be explained by a small number of experimental points for $L < 60$ cm and by poor accuracy of the transmission measurements. Thus, more accurate transmission measurements at an increased number of sample lengths are needed to justify the proposed scaling of transmission quantities in localized samples in the presence of absorption.

4.3 Distribution of transmitted intensity of localized waves

In the localized regime $L \geq \xi$, the fluctuations in transmission quantities are much larger than the average. In the absence of absorption, in the localization limit $L \gg \xi$, distributions of all transmission quantities were predicted to be log-normal [119, 120]. Here we consider the distribution of transmitted intensity for localized waves in lossy alumina samples.

The distribution of the normalized intensity, $P(s_{ab})$, for alumina samples with $L = 90$ cm is shown by squares in Fig. 4.6a, using a semi-logarithmic scale. The solid line is the fit of the diffusive result [33, 34], $P(s_{ab}) \sim \exp(-2\sqrt{g' s_{ab}})$, derived for $g' \gg 1$, to the tail of the distribution, for $s_{ab} > 30$. The fit gives $g' = 0.162$, which is close to $g' = 2/3var(s_a) = 7/3var(s_{ab}) = 0.154$. A good fit to the tail of the distribution and good agreement between values of g', obtained from the fit and from $var(s_{ab})$, show that the stretched exponential tail of the intensity distribution,

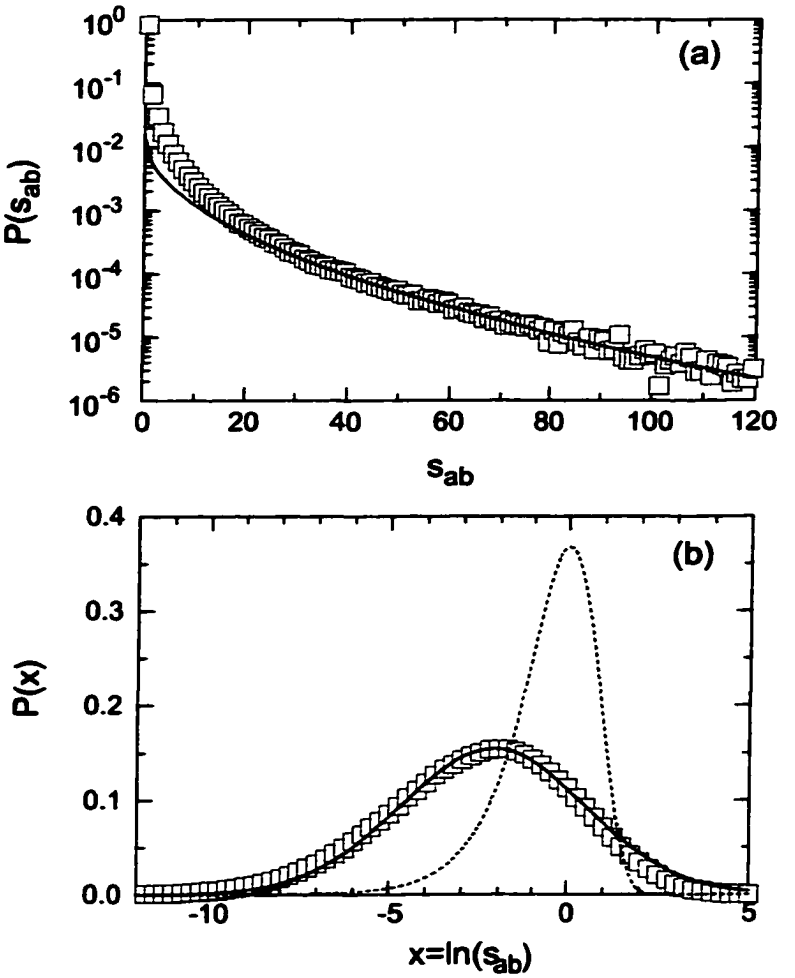

Figure 4.6: (a) The distribution of the normalized intensity, $P(s_{ab})$, in the frequency interval 9.94-10.10 GHz, for alumina samples with $L = 90$ cm (squares), and the fit to the tail of this distribution with the theoretical result [33, 34], $P(s_{ab}) \sim \exp(-2\sqrt{g' s_{ab}})$ (solid). The value of the fitting parameter is $g' = 0.162$. (b) The distribution of the logarithm of the normalized intensity, $P(\ln s_{ab})$, for the same samples (squares) and the fit of the log-normal distribution [119, 120], $P(x = \ln s_{ab}) \propto \exp[-\xi(x - \langle x \rangle)^2/8L]$ to the bulk of this distribution (solid). The fit gives the localization length, $\xi = 53.2$. The dashed curve is the distribution, $P(x) = \exp[x - \exp(x)]$, corresponding to the diffusion limit, $g \to \infty$.

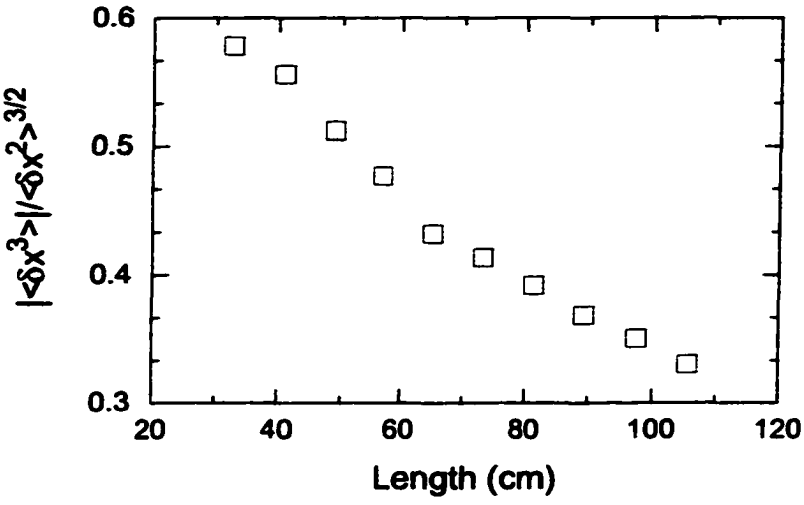

Figure 4.7: Scaling of the absolute value of the skewness coefficient, $|\mu| = |\langle \delta x^3 \rangle| / \langle \delta x^2 \rangle^{3/2}$, of the distribution $P(x = \ln s_{ab})$ in alumina samples. The frequency range is 9.94-10.1 GHz.

$P(s_{ab}) \sim \exp(-2\sqrt{g' s_{ab}})$, may still be a good approximation for $P(s_{ab})$, for $s_{ab} \gg 1$, even in samples with sample length $L \geq \xi$.

The distribution of the logarithm of the normalized intensity, $P(\ln s_{ab})$, for the same samples is displayed by the squares in Fig. 4.6b. The solid line is now the fit of the normal distribution [119, 120], $P(x = \ln s_{ab}) \propto \exp[-\xi(x - \langle x \rangle)^2 / 8L]$, to the bulk of the distribution $P(\ln s_{ab})$. The value of the fitting parameter is $\xi = 53.2$ cm, which is close to the values $\xi = 60.0$ cm and $\xi = 63.0$ cm, obtained from a consideration of the scaling of $\langle I_{ab} \rangle$, $\exp\langle \ln I_{ab} \rangle$ and $var(\ln I_{ab})$ in the previous section. The dashed line is the distribution of $x = \ln s_{ab}$ in the diffusive limit $g \to \infty$, $P(x) = \exp[x - \exp(x)]$, which is obtained from the Rayleigh distribution. In the transition from diffusive propagation to localization, the distribution $P(\ln s_{ab})$ is found to approach a normal distribution. The absolute value of the coefficient of skewness of the distribution $P(x = \ln s_{ab})$, $|\mu| = |\langle \delta x^3 \rangle| / \langle \delta x^2 \rangle^{3/2}$, as a function of sample length L, is shown in Fig. 4.7. As the sample length increases, $|\mu|$ decreases linearly, with a kink near $L \approx 60$ cm, which is the localization threshold.

CHAPTER 5
STATISTICS OF DYNAMICS OF LOCALIZED WAVES

In this chapter, we consider the dynamic statistics of localized waves. The joint statistics of the transmitted intensity and single-channel delay time, as well as the statistics of the delay times, of microwave radiation within a window of localization, in samples of randomly positioned alumina spheres, are compared to those for extended waves in a different frequency interval in the same samples.

We measure the microwave field transmission coefficient $\sqrt{I_{ab}}\exp(i\phi_{ab})$ in ensembles of alumina samples. The amplitude $\sqrt{I_{ab}}$ and the phase ϕ_{ab} of the field at the output surface, referenced to the field at the input surface, are obtained using a Hewlett-Packard HP8722C vector network analyzer. Alumina spheres of diameter 0.95 cm and dielectric constant 9.86 are contained in a 7.3-cm-diameter copper tube at a volume fraction of 0.068. This low density is achieved by embedding the alumina spheres in 1.9-cm-diameter Styrofoam spheres with dielectric constant 1.08. The measurements are carried out in samples of length 49, 65, and 90 cm.

The degree of localization in these samples is given by the variance of the total transmission normalized to its ensemble average value, $var(s_a)$. Calculated values of $var(s_a)$, as well as measurements of scaling of $var(s_a)$ and $\langle I_{ab}\rangle$ with sample length, allowed us to establish that the wave is localized in a narrow frequency range centered at $f \approx 10$ GHz and that the wave is extended outside this range. Here we compare the dynamic statistics in the frequency interval of 9.94-10.1 GHz, within the window of localization, to those for extended waves in the interval of 16.9-17 GHz near the fourth Mie resonance of the alumina spheres. These frequency intervals are sufficiently narrow that within them propagation parameters are nearly constant.

The probability distributions $P(\widehat{\phi}')$ of the normalized single-channel delay time in a sample of $L = 90$ cm are shown in Fig. 5.1. The ensemble-averaged values of ϕ'_{ab} within the lower and upper frequency intervals are 122 and 120 ns, respectively. The

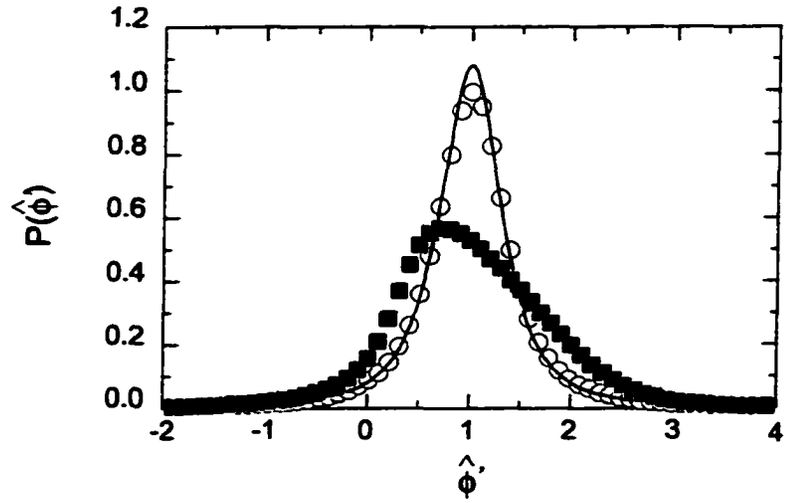

Figure 5.1: Probability distribution of the normalized delay time for extended (circles) and localized (squares) waves in a sample of $L = 90$ cm. The curve is the distribution $P(\hat{\phi}')$ in the diffusive limit [61, 62], given by Eq. 1.4 with $Q = 0.215$.

values of $var(s_a)$ at these frequencies are, respectively, 7.1 and 0.37, indicating that radiation is localized in the lower frequency interval and extended in the upper interval, though the intensity correlation is high. The distribution $P(\hat{\phi}')$ for extended waves is compared to that in the diffusive limit [61, 62], given by Eq. 1.4. Measurements of the scaling of $\langle I_{ab} \rangle$ with sample length for extended waves yield $L_a = 21.3 \pm 1.6$ cm, which translates into $Q = 0.215$. This value is substituted in Eq. 1.4 to produce the curve in Fig. 5.1. We note, however, that a fit of Eq. 1.4 to the data using Q as a fitting parameter gives $Q = 0.249$, which corresponds to $L_a = 26.0 \pm 0.4$ cm. The underestimate of absorption, resulting from the fit of Eq. 1.4, indicates the beginning of a breakdown of the diffusion theory of [61, 62], which is expected in strongly correlated samples. In contrast, the normalized delay time distribution for localized waves bears little resemblance to the predictions of diffusion theory. It is asymmetrical and reaches its peak at a value of $\hat{\phi}'$ below its average value of unity.

We find further that the conditional probability distribution $P_{\hat{I}}(\hat{\phi}')$ for a fixed value of $\hat{I}$ for extended waves is well described by a gaussian for any $\hat{I}$ and L, in

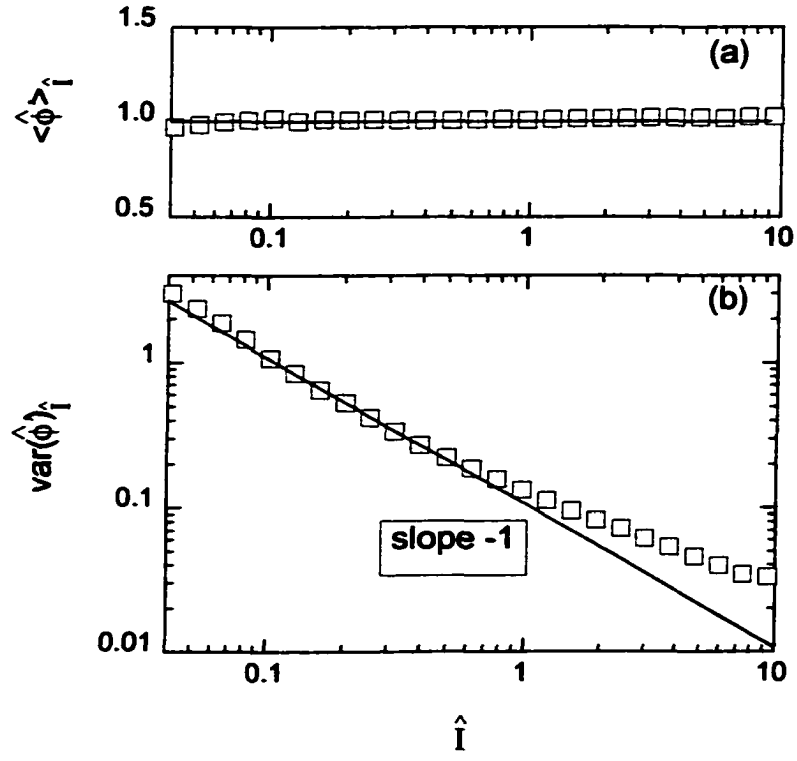

Figure 5.2: Variation with $\hat{I}$ of (a) $\langle\hat{\phi}'\rangle_{\hat{I}}$ and (b) $var(\hat{\phi}')_{\hat{I}}$ for extended waves for $L = 90$ cm. The lines in (a) and (b) are the diffusive limits [61, 62], $\langle\hat{\phi}'\rangle_{\hat{I}} = 1$ and $var(\hat{\phi}')_{\hat{I}} = Q/2\hat{I}$, respectively, with $Q = 0.215$.

agreement with the diffusion theory. The variation of $\langle\hat{\phi}'\rangle_{\hat{I}}$ and $var(\hat{\phi}')_{\hat{I}}$ upon $\hat{I}$ in a sample of $L = 90$ cm is shown in Fig. 5.2. Whereas $\langle\hat{\phi}'\rangle_{\hat{I}}$ is, as expected, nearly independent of $\hat{I}$ (Fig. 5.2a), $var(\hat{\phi}')_{\hat{I}}$ shows a departure from the prediction for diffusive waves of $Q/2\hat{I}$, for $\hat{I} > 0.5$ (Fig. 5.2b). This is consistent with the deviation of the distribution $P(\hat{\phi}')$ for extended waves from diffusion theory, seen in Fig. 5.2.

In contrast to the gaussian distribution found for extended waves, the conditional probability distribution $P_{\hat{I}}(\hat{\phi}')$ for localized waves exhibits an exponential fall-off, with an asymmetry in the distribution, which increases with decreasing $\hat{I}$ (Fig. 5.3). The variation of $\langle\hat{\phi}'\rangle_{\hat{I}}$ and $var(\hat{\phi}')_{\hat{I}}$ with $\hat{I}$ for different values of L is presented in

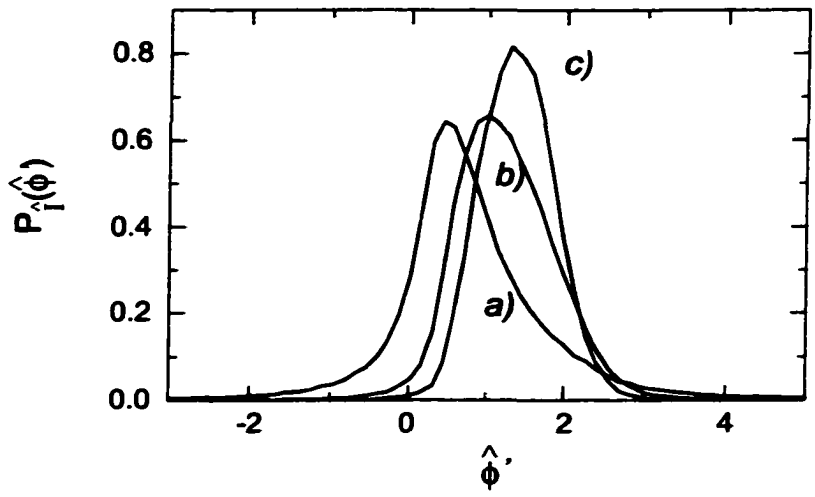

Figure 5.3: Conditional probability distribution $P_{\hat{I}}(\hat{\phi}')$ for the values of $\hat{I}$ of 0.04 (a), 0.4 (b), and 4.0 (c) for localized waves for $L = 90$ cm.

Fig. 5.4. As seen in Fig. 5.4a, $\langle\hat{\phi}'\rangle_{\hat{I}}$ markedly increases with $\hat{I}$ to an extent, which increases with L. The variation of $var(\hat{\phi}')_{\hat{I}}$, seen in Fig. 5.4b, is even more striking. For all sample lengths, we find that for $\hat{I} > 0.5$, $var(\hat{\phi}')_{\hat{I}}$ converges to $q/(\hat{I})^{1/4}$, with $q = 0.4$, shown as the line in Fig. 5.4b. This universal behavior at large $\hat{I}$ suggests a similarity in the dynamics of localized and prelocalized states [68, 121, 122]. For smaller values of $\hat{I}$, $var(\hat{\phi}')_{\hat{I}}$ becomes smaller and falls more slowly with $\hat{I}$, as sample length increases. For $L = 90$ cm, $var(\hat{\phi}')_{\hat{I}} = 0.4/(\hat{I})^{1/4}$ for any $\hat{I}$.

The probability distributions of the normalized weighted delay time, $\widehat{W} \equiv W_{ab}/\langle W_{ab}\rangle$, for extended and localized waves for $L = 90$ cm are compared in Fig. 5.5. The dashed line is the predicted double-sided exponential distribution in the diffusive limit [61, 62], given by Eq. 1.5 with $Q = 0.215$ found in the upper frequency interval. The distribution for extended waves, however, is seen to deviate significantly from diffusion theory, indicating the sensitivity of this distribution to approaching localization. For localized waves, the distribution is considerably broader. It is well approximated by a double-sided stretched exponential, $P(\widehat{W}) = a\exp(-b|\widehat{W}|^{1/3})$, with $a = 0.44$ and $b = 2.42$ for $\widehat{W} > 0$, and $a = 0.07$ and $b = 5.50$ for $\widehat{W} < 0$, shown

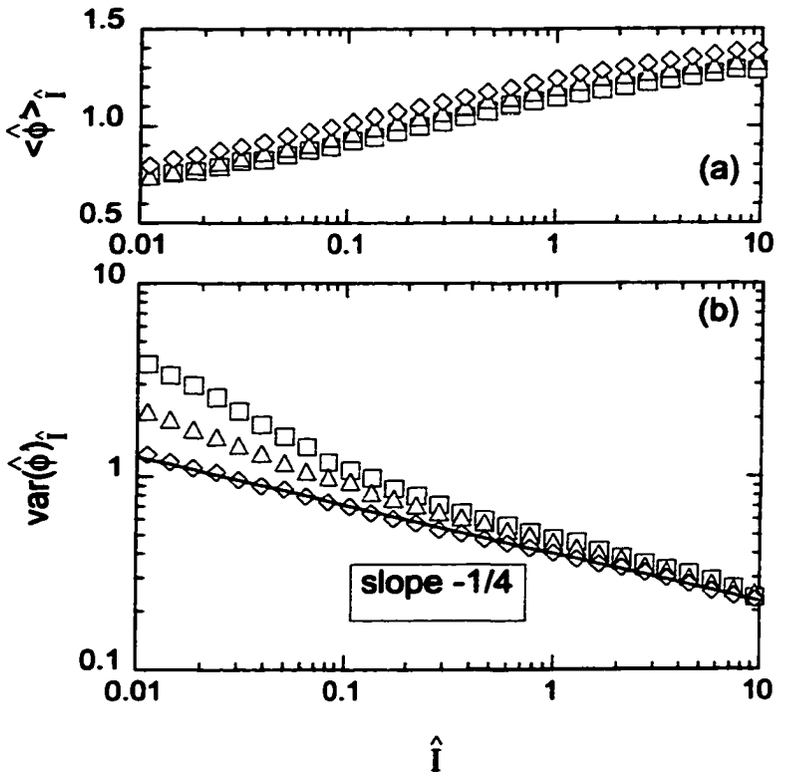

Figure 5.4: Variation with $\hat{I}$ of (a) $\langle\hat{\phi}'\rangle_{\hat{I}}$ and (b) $var(\hat{\phi}')_{\hat{I}}$ for localized waves for $L = 49$ cm (squares), 65 cm (triangles), and 90 cm (diamonds). The line in (b) is $var(\hat{\phi}')_{\hat{I}} = q/(\hat{I})^{1/4}$, with $q = 0.4$.

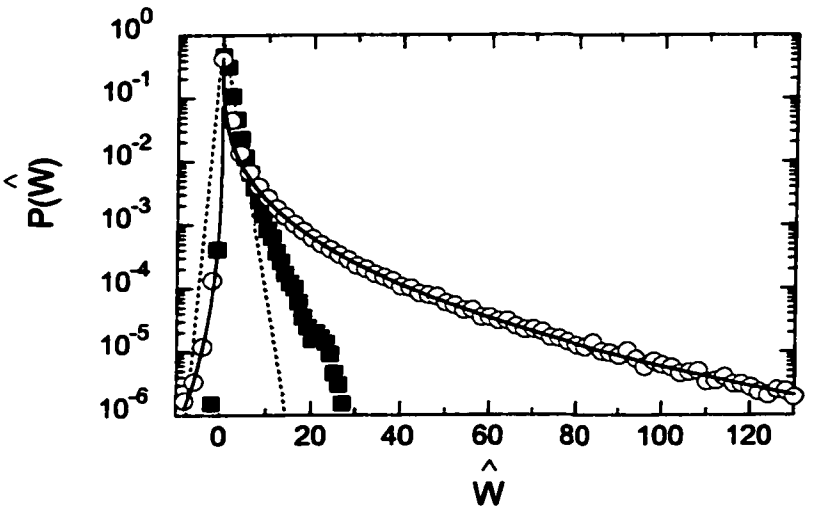

Figure 5.5: Probability distribution of the normalized weighted delay time for extended (squares) and localized (circles) waves for $L = 90$ cm. The dashed line is the distribution $P(\widehat{W})$ in the diffusive limit [61, 62], with $Q = 0.215$. The solid line is the model distribution, $P(\widehat{W}) = a\exp(-b|\widehat{W}|^{1/3})$, with $a = 0.44$ and $b = 2.42$ for $\widehat{W} > 0$, and $a = 0.07$ and $b = 5.50$ for $\widehat{W} < 0$.

as the solid line in Fig. 5.5. The distribution of $\widehat{W}$ is wider than that of $\widehat{I}$, reflecting the enhanced probability of long dwell times and the increased variance of dwell times at large values of the intensity for localized waves.

We have previously shown that $var(\widehat{I})$, as well as $var(s_a)$, serve as indicators of localization, even in the presence of absorption [44, 104]. We find that the interaction between dynamic and static statistics associated with $\widehat{\phi'}$ and $\widehat{I}$, respectively, may also be used to identify the range of localization. The correlation between $\widehat{I}$ and $\widehat{\phi'}$ can be expressed as the dimensionless ratio, $\langle \widehat{I}\,\widehat{\phi'} \rangle \equiv \langle I_{ab}\phi'_{ab} \rangle / \langle I_{ab} \rangle \langle \phi'_{ab} \rangle$. The frequency variation of this ratio in a sample of $L = 80$ cm is plotted in Fig. 5.6. It is unity in the diffusive limit, since $P_{\widehat{I}}(\widehat{\phi'})$ is then a gaussian centered at $\langle \widehat{\phi'} \rangle_{\widehat{I}} = 1$, and rises above unity, as localization is approached. The variation with frequency of $\langle \widehat{I}\,\widehat{\phi'} \rangle$ follows closely that of $var(\widehat{I})$ (see Fig. 3.2). The localization threshold, at which $var(\widehat{I}) = 7/3$ [104], corresponds to the condition, $\langle \widehat{I}\,\widehat{\phi'} \rangle = 1.1$, shown as the dotted line in Fig. 5.6.

In conclusion, we find striking differences between the statistics of dynamics of localized and extended waves. Characteristic features of the statistics of localized waves are an increasing average delay time with intensity, an asymptotic decay of the variance of the delay time proportional to $1/(\widehat{I})^{1/4}$, and a double-sided stretched exponential distribution of the weighted delay time. These features reflect transport via resonant coupling to isolated localized states. We expect that the distinctive and complex behavior observed is characteristic of electron transport as well as of propagation of all varieties of classical waves.

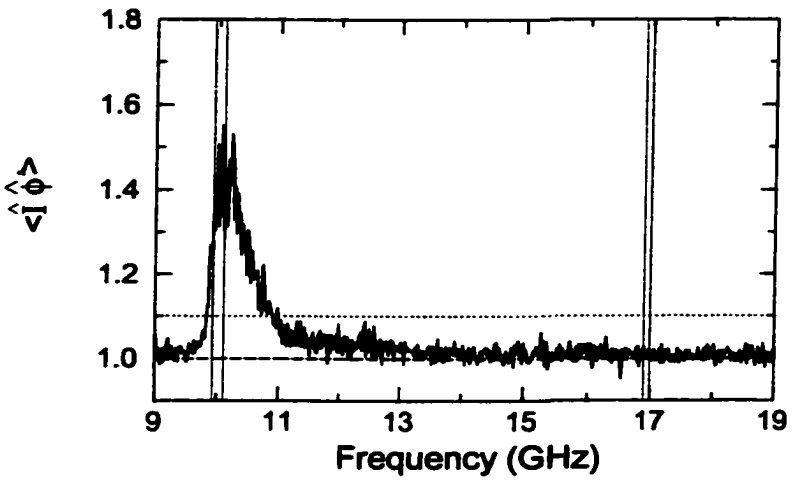

Figure 5.6: Dimensionless ratio, $\langle \widehat{I}\,\widehat{\phi'} \rangle \equiv \langle I_{ab}\phi'_{ab} \rangle / \langle I_{ab} \rangle \langle \phi'_{ab} \rangle$, versus frequency for $L = 80$ cm. The dashed line corresponds to the value of unity of this ratio in the diffusive limit [61, 62]. The dotted line represents the condition, $\langle \widehat{I}\,\widehat{\phi'} \rangle = 1.1$, which corresponds to the localization criterion, $var(\widehat{I}) = 7/3$ [104]. The peak above this line indicates the window of localization. The frequency intervals used in computing the statistics for localized and extended waves in Figs. 5.1-5.5 are marked by vertical lines.

CHAPTER 6
SUMMARY

The presence of large fluctuations in wave propagation in random media points to the need for a statistical description. The nature of fluctuations is determined by the closeness to the localization transition. In the absence of absorption, this can be specified, in many circumstances, by a single parameter – the ensemble average of the dimensionless conductance, g. As a result, the extent of localization can be determined by any of a wide variety of related statistical measurements. Among the quantities that most directly reflect key aspects of localization are the following: (i) the ensemble average of the dimensionless conductance g, (ii) the ratio of the width to the spacing of modes of an open sample, $\delta = \delta\nu/\Delta\nu$, and (iii) a new parameter – the variances of the probability distribution of transmission quantities, such as the intensity, the total transmission, and the dimensionless conductance. We show that these quantities in low-density collections of alumina spheres in a quasi-1D geometry are equivalent measures of localization for $L < L_a, \xi$.

We find that even in the presence of absorption, the extent of localization can be characterized by a single parameter – the variance of the total transmission normalized by its ensemble average, $var(s_a)$. Measurements of fluctuations in intensity and total transmission of microwave radiation allow us to study photon localization in both weakly and strongly scattering quasi-1D dielectric samples and in periodic metallic wire meshes containing metallic scatterers, while ruling it out in three-dimensional samples of aluminum spheres. In low-density collections of alumina spheres contained in an open copper tube, we find that, at frequencies near the first Mie resonance, the variance of normalized total transmission scales exponentially once it becomes greater than unity. Localization appears in these samples as a result of collective resonant scattering. It does not occurs on resonance, though, because the narrowing of the level width $\delta\nu$ is offset by the enhancement of the density of state $N(\nu)$, corresponding to

a reduction in the level spacing $\Delta\nu$. However, a sharp drop in $N(\nu)$ above resonance results in a minimum in δ and the consequent appearance of localization.

When $var(s_{ab})$ is large, transmission spectra are observed to be a series of narrow lines with widths that are smaller than the separation between peaks. The appearance of sharp transmission lines is the result of resonant transmission through localized states. When the frequency of the incident wave is tuned into resonance with a localized state, transmission is appreciable; otherwise, it is small as a result of evanescent coupling. An isolated transmission line is shown to have a Lorentzian form. These spectra have an extraordinarily wide intensity distribution. As localization becomes stronger in longer samples, the intensity distribution approaches a log-normal distribution.

The statistics of dynamics of localized waves are profoundly different from that for extended waves, as a result of resonant transmission. The distribution of the single-channel delay time becomes markedly asymmetric, while the distribution of the delay time weighted by intensity becomes extraordinarily broad. The latter falls as a stretched exponential to the power 1/3 instead of exponentially, as predicted for diffusing waves. The average normalized delay time at fixed intensity, $\langle\widehat{\phi}'\rangle_{\widehat{I}}$, which is independent of $\widehat{I}$ for diffusive waves, is found to increase with $\widehat{I}$. At the same time, the decrease with intensity of the variance of the normalized delay time is substantially reduced. As a result, the delay time and intensity are correlated and afford a dynamical test for localization.

The research presented in this thesis show that the statistics of transmission are essential aspects of electromagnetic propagation and localization.

REFERENCES

[1] A. Ishimaru, *Wave Propagation and Scattering in Random Media* (Academic Press, New York, 1978).

[2] J.W. Goodman, *Statistical Optics* (Wiley, New York, 1985).

[3] *Scattering and Localization of Classical Waves in Random Media*, edited by P. Sheng (World Scientific Press, Singapore, 1990).

[4] *Mesoscopic Phenomena in Solids*, edited by B.L. Altshuler, P.A. Lee, and R.A. Webb (Elsevier, Amsterdam, 1991).

[5] *Diffuse Waves in Complex Media*, edited by J.-P. Fouque (Kluwer Academic Publishers, Dordrecht, 1999).

[6] *Waves and Imaging through Complex Media*, edited by P. Sebbah (Kluwer Academic Publishers, Dordrecht, 2001).

[7] I. Freund and D. Elyahu, Phys. Rev. A **45**, 6133 (1992).

[8] A.Z. Genack, Phys. Rev. Lett. **58**, 2043 (1987).

[9] A.Z. Genack and J.M. Drake, Europhys. Lett. **11**, 331 (1990).

[10] J.W. Strutt (Lord Rayleigh), Proc. Lond. Math. Soc. **3**, 267 (1871).

[11] J.C. Dainty, *Laser Speckle and Related Phenomena* (Springer-Verlag, Berlin, 1975).

[12] R.A. Webb, S. Washburn, C.P. Umbach, and R.B. Laibowitz, Phys. Rev. Lett. **54**, 2696 (1985).

[13] B.L. Altshuler and D.E. Khmelnitskii, JETP Lett. **42**, 359 (1985).

[14] P.A. Lee and A.D. Stone, Phys. Rev. Lett. **55**, 1622 (1985).

[15] B. Shapiro, Phys. Rev. Lett. **57**, 2168 (1986).

[16] B. Shapiro, Phil. Mag. B **56**, 1031 (1987).

[17] M.J. Stephen and G. Cwilich, Phys. Rev. Lett. **59**, 285 (1987).

[18] G. Maret and P.E. Wolf, Z. Phys. B **65**, 409 (1987).

[19] P.A. Mello, E. Akkermans, and B. Shapiro, Phys. Rev. Lett. **61**, 459 (1988).

[20] S. Feng, C. Kane, P.A. Lee, and A.D. Stone, Phys. Rev. Lett. **61**, 834 (1988).

[21] I. Edrei, M. Kaveh, and B. Shapiro, Phys. Rev. Lett. **62**, 2120 (1989).

[22] R. Pnini and B. Shapiro, Phys. Rev. B **39**, 6986 (1989).

[23] N. Garcia and A.Z. Genack, Phys. Rev. Lett. **63**, 1678 (1989).

[24] A.Z. Genack, N. Garcia, and W. Polkosnik, Phys. Rev. Lett. **65**, 2129 (1990).

[25] M.P. van Albada, J. F. de Boer, and A. Lagendijk, Phys. Rev. Lett. **64**, 2787 (1990).

[26] N. Shnerb and M. Kaveh, Phys. Rev. B **43**, 1279 (1991).

[27] E. Kogan and M. Kaveh, Phys. Rev. B **45**, 1049 (1992).

[28] E. Kogan, M. Kaveh, R. Baumgartner, and R. Berkovits, Phys. Rev. B **48**, 9404 (1993).

[29] A. Z. Genack and N. Garcia, Europhys. Lett. **21**, 753 (1993).

[30] N. Garcia, A.Z. Genack, R. Pnini, and B. Shapiro, Phys. Lett. A **176**, 458 (1993).

[31] R. Berkovits and S. Feng, Phys. Rep. **238**, 135 (1994).

[32] J.F. de Boer, M.C.W. van Rossum, M.P. van Albada, Th.M. Nieuwenhuizen, and A. Lagendijk, Phys. Rev. Lett. **73**, 2567 (1994).

[33] M.C.W. van Rossum and Th.M. Nieuwenhuizen, Phys. Rev. Lett. **74**, 2674 (1994).

[34] E. Kogan and M. Kaveh, Phys. Rev. B **52**, R3813 (1995).

[35] V. Fal'ko and K. Efetov, Phys. Rev. B **52**, 17413 (1995).

[36] S.A. van Langen, P.W. Brouwer, and C.W.J. Beenakker, Phys. Rev. E **53**, 1344 (1996).

[37] A.A. Chabanov and A.Z. Genack, Phys. Rev. E **56** R1338 (1997).

[38] M. Stoytchev and A.Z. Genack, Phys. Rev. Lett. **79** 309 (1997).

[39] P.W. Brouwer, Phys. Rev. B, **57**, 10526 (1998).

[40] F. Scheffold and G. Maret, Phys. Rev. Lett. **81**, 5800 (1998).

[41] M. Stoytchev and A.Z. Genack, Opt. Lett. **24**, 262 (1999).

[42] M.C.W. van Rossum and Th.M. Nieuwenhuizen, Rev. Mod. Phys. **71**, 313 (1999).

[43] M. Stoytchev, Ph.D. Thesis (City University of New York, 1998).

[44] A.A. Chabanov, M. Stoytchev, and A.Z. Genack, Nature **404**, 850 (2000).

[45] P. Sebbah, R. Pnini, and A.Z. Genack, Phys. Rev. E **62**, 7348 (2000).

[46] R. Pnini, in *Waves and Imaging through Complex Media*, edited by P. Sebbah (Kluwer Academic Publishers, Dordrecht, 2001).

[47] L. Eisenbud, Ph.D thesis, Princeton University, 1948.

[48] E. Wigner, Phys. Rev. **98**, 145 (1955).

[49] F.T. Smith, Phys. Rev. **118**, 349 (1960); **119**, 2098 (1960).

[50] B. White, P. Sheng, Z.Q. Zhang, and G. Papanicolaou, Phys. Rev. Lett. **59**, 1918 (1987).

[51] M. Büttiker, H. Thomas, and A. Pretre, Phys. Lett. A **180**, 364 (1993).

[52] J.G. Muga and D.M. Wardlaw, Phys. Rev. E **51**, 5377 (1995).

[53] P. Šeba, K. Zyczkowski, and J. Zakrewski, Phys. Rev. E **54**, 2438 (1996).

[54] Y.V. Fyodorov and H.J. Sommers, Phys. Rev. Lett. **76**, 4709 (1996).

[55] V.A. Gopar, P.A. Mello, and M. Büttiker, Phys. Rev. Lett. **77**, 3005 (1996).

[56] P.W. Brouwer, K.M. Frahm, and C.W.J. Beenakker, Phys. Rev. Lett. **78**, 4737 (1997).

[57] P. Sebbah, O. Legrand, B.A. van Tiggelen, and A.Z. Genack, Phys. Rev. E **56**, 3619 (1997).

[58] P. Sebbah, O. Legrand, and A.Z. Genack, Phys. Rev. E **59**, 2406 (1999).

[59] C. Texier and A. Comtet, Phys. Rev. Lett. **82**, 4220 (1999).

[60] G. Iannacone, Phys. Rev. B **51**, 4727 (1995).

[61] A.Z. Genack, P. Sebbah, M. Stoytchev, and B.A. van Tiggelen, Phys. Rev. Lett. **82**, 715 (1999).

[62] B.A. van Tiggelen, P. Sebbah, M. Stoytchev, and A.Z. Genack, Phys. Rev. E **59**, 7166 (1999).

[63] M. Titov and C.W.J. Beenakker, Phys. Rev. Lett. **85**, 3388 (2000).

[64] H. Schomerus, K.J.H. van Bemmel, and C.W.J. Beenakker, Phys. Rev. E **63**, 26605 (2001).

[65] C.W.J. Beenakker, in *Photonic Crystals and Light Localization in the 21st Century*, edited by C.M. Soukoulis, (Kluwer, Dordrecht, 2001).

[66] H. Schomerus, Phys. Rev. E **64**, 26606 (2001).

[67] A.A. Chabanov and A.Z. Genack, Phys. Rev. Lett. **87**, 233903 (2001).

[68] B.L. Altshuler, V.E. Kravtsov, and I.V. Lerner, *Mesoscopic Phenomena in Solids*, edited by B.L. Altshuler, P.A. Lee, and R.A. Webb (Elsevier, Amsterdam, 1991).

[69] J.-L. Pichard in *Waves and Imaging through Complex Media*, edited by P. Sebbah (Kluwer Academic Publishers, Dordrecht, 2001).

[70] P.W. Anderson, Phys. Rev. **109**, 1492 (1958).

[71] J.T. Edwards and D.J. Thouless, J. Phys. **C5**, 807 (1972).

[72] A.Z. Genack, Europhys. Lett. **11**, 733 (1990).

[73] D.J. Thouless, Phys. Rev. Lett. **39**, 1167 (1977).

[74] E. Abrahams, P.W. Anderson, D.C. Licciardello, and T.V. Ramakrishnan, Phys. Rev. Lett. **42**, 673 (1979).

[75] S. John, H. Sompolinsky, and M.J. Stephen, Phys. Rev. B **27**, 5592 (1983).

[76] S. John, Phys. Rev. Lett. **53**, 2169 (1984).

[77] R. Landauer, Phil. Mag. **21**, 863 (1970).

[78] D.S. Fisher and P.A. Lee, Phys. Rev. B **23**, 6851 (1981).

[79] B.A. van Tiggelen, in *Diffuse Waves in Complex Media*, edited by J.-P. Fouque (Kluwer Academic Publishers, Dordrecht, 1999).

[80] M.P. van Albada, B.A. van Tiggelen, A. Lagendijk, and A. Tip, Phys. Rev. Lett. **66**, 3132 (1991).

[81] A. Lagendijk and B.A. van Tiggelen, Phys. Rep. **270**, 143 (1996).

[82] Y. Kuga and A. Ishimaru, J. Opt. Soc. Am. **A1**, 831 (1984).

[83] M. van Albada and A. Lagendijk, Phys. Rev. Lett. **55**, 2692 (1985).

[84] P.F. Wolf and G. Maret, Phys. Rev. Lett. **55**, 2696 (1985).

[85] E. Akkermans, P.E. Wolf, and R. Maynard, Phys. Rev. Lett. **56**, 1471 (1986).

[86] A.F. Ioffe and A.R. Regel, Prog. Semicond. **4**, 237 (1960).

[87] R.L. Weaver, Phys. Rev. B **47**, 1077 (1993).

[88] V. Freilikher, M. Pustilnik, and I. Yurkevich, Phys. Rev. Lett. **73**, 810 (1994).

[89] M. Yosefin, Europhys. Lett. **25**, 675 (1994).

[90] J.C.J. Paasschens, T.Sh. Mizirpashaev, and C.W.J. Beenakker, Phys. Rev. B **54**, 11887 (1996).

[91] N. Garcia and A.Z. Genack, Phys. Rev. Lett. **66**, 1850 (1991).

[92] A.Z. Genack and N. Garcia, Phys. Rev. Lett. **66**, 2064 (1991).

[93] D.S. Wiersma, P. Bartolini, A. Lagendijk, and R. Righini, Nature, **390**, 671 (1997);

[94] D.S. Wiersma, J.G. Rivas, P. Bartolini, A. Lagendijk, and R. Righini, Nature **398**, 207 (1999).

[95] F. Scheffold, R. Lenke, R. Tweer, and G. Maret, Nature **398**, 206 (1999).

[96] Yu.A. Vlasov, M.A. Kaliteevski, and V.V. Nikolaev, Phys. Rev. B **60**, 1555 (1999).

[97] B.A. van Tiggelen, A. Lagendijk, and D.S. Wiersma, Phys. Rev. Lett. **84**, 4333 (2000).

[98] P.W. Anderson, D.J. Thouless, E. Abrahams, and D.S. Fisher, Phys. Rev. B **22**, 3519 (1980).

[99] P.A. Mello, J. Math. Phys. (N. Y.) **27**, 2876 (1986).

[100] L.I. Deych, D. Zaslavsky, and A.A. Lisyansky, Phys. Rev. Lett. **81**, 5390 (1998).

[101] L.I. Deych, A.A. Lisyansky, and B.L. Altshuler, Phys. Rev. Lett. **84**, 2678 (2000).

[102] N. Garcia, A.Z. Genack, and A.A. Lisyansky, Phys. Rev. B **46**, 14475 (1992).

[103] A. Lagendijk, R. Vreeker, and P. de Vries, Phys. Lett. A **136**, 81 (1989).

[104] A.A. Chabanov and A.Z. Genack, Phys. Rev. Lett. **87**, 153901 (2001).

[105] S. John, Phys. Rev. Lett. **58**, 2486 (1987).

[106] J.D. Joannopolos, R.D. Meade, and J.N. Winn, *Photonic Crystals* (Princeton University Press, Princeton, 1995).

[107] M. Stoytchev and A.Z. Genack, Phys. Rev. B **55**, R8617 (1997).

[108] K. Arya, Z.B. Su, and J.L. Birman, Phys. Rev. Lett. **57**, 2725 (1986).

[109] C.A. Condat and T.R. Kirkpatrik, Phys. Rev. Lett. **58**, 226 (1987).

[110] A. Lagendijk, in *Current Trends in Optics*, edited by J.C. Dainty (Academic, London, 1994).

[111] F.J.P. Schuurmans, M. Megens, D. Vanmaekelbergh, and A. Lagendijk, Phys. Rev. Lett. **83**, 2183 (1999).

[112] Y. Imry, Europhys. Lett. **1**, 247 (1986).

[113] M.Ya. Azbel, Solid State Commun. **45**, 527 (1983).

[114] A.B. Fowler, A. Hartstain, and R.A. Webb, Phys. Rev. Lett. **48**, 196 (1982).

[115] R.F. Kwasnick, M.A. Kastner, J. Melngailis, and P.A. Lee, Phys. Rev. Lett. **52**, 224 (1984).

[116] P.A. Lee, Phys. Rev. Lett. **53**, 2042 (1984).

[117] P.W. Brouwer, Phys. Rev. B **57**, 10526 (1998).

[118] C.W.J. Beenakker, Rev. Mod. Phys. **69**, 731 (1997).

[119] J.-L. Pichard and M. Sanquer, Physica A **167**, 66 (1990).

[120] S.A. van Langen, P.W. Brouwer, and C.W.J. Beenakker, Phys. Rev. E **53**, R1344 (1996).

[121] V.I. Falko and K.B. Efetov, Phys. Rev. B **52**, 17413 (1995).

[122] A.D. Mirlin, Phys. Rev. B **53**, 1186 (1996).